CHAPTER 4

Metals in Alzheimer's Disease: A Combined Experimental and Numerical Approach

Silvia Morante* **and Giancarlo Rossi**

Dipartimento di Fisica, Università di Roma "Tor Vergata" and INFN, Sezione di Roma "Tor Vergata", Via della Ricerca Scientifica, 00133 Roma, Italy

Abstract: Alzheimer disease is a pathology causing severe problems with memory, thinking and behavior. It accounts for the majority of dementia cases and is the sixth leading cause of death in developed countries. Unfortunately a real cure is still missing and the drug treatments today available can only reduce symptoms. It belongs to a large class of diseases, called amyloidosis, in which endogenous proteins or peptides undergo a misfolding process switching from the physiological soluble configuration to a pathological fibrillar insoluble state. An important, but not yet fully elucidated, rôle appears to be played in these processes by transition metals (mainly copper and zinc) that have been observed to be present in fairly large amounts in patient's neurological plaques. In this review we will show that the challenging problem of understanding the physico-chemical basis of protein misfolding and aggregation can be successfully investigated with a combination of modern spectroscopic techniques and advanced *first principle* numerical simulations. In particular, it will be shown that different metals can rival in peptide binding thus adding support to the hypothesis that metal dyshomeostasis may be relevant in the Alzheimer disease development.

Keywords: Amyloidosis, Aβ-peptide, *ab initio* molecular dynamics, metal ions, X-ray Absorption Spectroscopy.

1. INTRODUCTION

Although the discovery of the presence of iron-containing compounds in blood can be traced back to the beginning of the 19th century, it is not more than fifty years that chemistry started a systematic study of rôle of metals in biology, that eventually led to the opening of a new branch of chemistry nowadays called "bioinorganic chemistry".

***Corresponding author Silvia Morante:** Dipartimento di Fisica, Università di Roma "*Tor Vergata*", INFN, Sezione di Roma "*Tor Vergata*", *Via* della Ricerca Scientifica, 00133 Roma, Italy; Tel: +390672594554; Fax: +39062023507; E-mail: silvia.morante@roma2.infn.it

D.K. Lahiri (Ed)

The 1950' renaissance of transition metal coordination chemistry was due to both the important new insights obtained from the application of ligand field theory [1] on the basic reaction mechanisms involving metal complexes, and to the increasing power of experimental and theoretical tools developed for the purpose of studying structural and kinetic properties of these biological systems at the molecular level.

Metals are electropositive elements characterized by ductility, malleability, brightness, and high conductance of heat and electricity. They can replace the hydrogen of an acid and form bases with hydroxyl radicals. Metals are not selective in their interaction with other molecules helping in a variety of important cellular events, such as chemical reaction catalysis, or electrons transport during energy production. On the other side, however, metal high chemical reactivity can easily become harmful, so sophisticated strategies for a careful tuning of their concentration have been evolutionarily developed in living organisms.

1.1.Metals and brain

Even in the brain metals like copper (Cu), zinc (Zn) and iron (Fe) are normally present at fairly high concentration and there are evidences that a breakdown in metal trafficking regulation (dyshomeostasis) has a significant impact in the development of age-related neurodegenerative diseases [2-4]. During neurotransmission processes high concentrations of Zn (at the level of ~300 μM) and Cu (at the level of ~30 μM) are normally released. Remarkably, release of Cu and Zn has been considered as one of the cause of the precipitation process (which starts in the synapse) leading to amyloid aggregation [5]. The concentration level of these metals was found to be, in fact, especially high in amyloid plaque deposits, reaching 0.4 mM in the case of Cu and 1 mM in the case of Zn [6].

Besides copper and zinc, many other metals (like calcium, magnesium, manganese, iron, cobalt, and molybdenum) are involved in the metabolism of the Central Nervous System (CNS), as catalysts, second messengers, gene expression regulators, *etc.*, and thus play an essential rôle in the correct functioning of the organ. Clearly metals must be supplied to the CNS in an optimally tuned way in order to prevent aberrant behaviours. The transport across the Blood Brain Barrier

(BBB) is the first step in the regulation of their level in the brain [7]. In this context it is interesting to note that high aluminium (Al) content was found in temporal cortex and hippocampus and that Al has been demonstrated to significantly alter the BBB permeability [8-10] with the consequence of accelerating amyloid aggregation [11]. Furthermore its *in vitro* co-incubation with either Zn^{2+} or Cu^{2+} ions was shown to promote precipitation, though possibly not amyloid fibrils formation [12].

In a recent structural study of metal binding to Prion Protein (PrP) [13], the misfolding and aggregation of which is the hallmark of Prion diseases, the existence of a possibly general mechanism for a Cu *vs.* Zn peptide binding competition has been demonstrated. This finding may be taken as an indirect confirmation of a (more general) correlation among failure of metal homeostasis, protein misfolding, and neurodegenerative disease development [14].

1.2. Amyloidosis and Neurodegenerative Diseases

The term *amyloidosis* indicates a family of pathologies caused by the transition of endogenous proteins and peptides from the physiological globular configuration to a (misfolded) harmful fibrillar state. It describes a heterogeneous group of diseases (more than 20) characterized by the extracellular deposition of fibrillar proteic material [15]. Regardless of the nature of the amyloid protein by which they are formed, fibrils have a common ultra-structure. They grow, unbranched, to a variable length that may reach several microns, with a diameter of 7-10 nanometers (1 nm $=10^{-9}$ meters). They are organized in a characteristic helicoidal β-structure and are able to bind to Congo Red and Thyoflavin dyes that are commonly used to detect their presence.

In many, if not in all, of the so-called neurodegenerative disorders, the phenomenon of abnormal protein aggregation is present. Among the many disorders with this aetiology in the present work we will focus our attention on the Alzheimer disease (AD). Our aim is to review some of the most recent structural studies on β-amyloid peptides (Aβ-peptides), whose aggregation is the hallmark of the AD development. The importance of any progress in understanding the biochemical basis of this devastating disease affecting an increasingly large

portion of the aged population [16], can hardly be underestimated, given the enormous medical and economical impact that AD has in the society.

1.2.1. Aβ-Peptides and Alzheimer's Disease

The typical AD amyloid plaques are formed by aggregates of Aβ-peptides. These are fragments that originate from the proteolytic cleavage of a membrane protein called Amyloid Precursor Protein (APP). They have a variable length between 39-43 residues owing to the heterogeneity of the cleavage position, localized at the C-terminus. The physiological rôle of cellular APP is still unknown.

The formation of AD plaques is a complex process: the proteolytic cleavage, performed by β- and γ-secretases, generates an intracellular pool of Aβ-peptides that may diffuse in the extracellular space. Soluble Aβ fragments assemble into small nascent β-amyloid fibrils with neurotoxic effects. Aβ fibrils deposit in cerebral tissues, forming highly ordered structures that constitute the nuclei of the typical plaques associated to the disease. At the basis of fibril formation there is a conformational change of the peptide that leads to the creation of an extended β-sheet like structure, capable of aggregating other peptides to form long antiparallel β-sheets with intra-molecular binding.

As we said, it has been observed that plaques contain large amounts of transition metals like Cu^{+2}, Fe^{+3} and Zn^{+2} (the latter being the most abundant). Their rôle is not yet fully understood but it has been conjectured to be crucial in the development of the AD pathology. The interest of elucidating the rôle of metals strongly increased after noticing that Cu^{+2} and Zn^{+2} chelators can be used to solubilize Aβ aggregates [17]. It is clear enough that the nature of the metal binding process can have significant consequences on the protein folding/unfolding and aggregation processes.

1.3. Content and Outline of the Review

The purpose of this review work is twofold. On the one hand we wish to present a fairly complete account of the important results that X-ray Absorption Spectroscopy (XAS) has provided in the years on the atomic structure of the metal binding site in Aβ-peptides metal complexes. On the other we want to discuss

how theoretical considerations, based on "*first principle*" simulations of realistic atomic models of these systems, can be of help in interpreting experimental data, thus leading to important insights into the physico-chemical properties of the metal-protein interaction.

The outline of the review is as follows. We start in sect. 2 with a general introduction on the XAS technique, that has been largely employed to investigate the geometry of the metal binding site in metal-protein complexes, and on the parallel complementary use of *ab initio* simulations developed to determine the detailed atomic structural arrangement characterizing not only the metallic site but also the peptide at large. In sect. 3 we describe in some detail the structural information that have been collected in the years, both through XAS (sect. 3.1) and through *ab initio* simulations (sect. 3.2), about the structure of the binding site of Cu and Zn, when these metals are in complex with Aβ-peptides. Conclusions and an outlook of future lines of investigations can be found in sect. 4. Few useful formulae are collected in two Appendices. The list of the abbreviations used in this review is given at the end of the main text.

2. EXPERIMENTAL AND THEORETICAL METHODS

Many experimental techniques have been employed during the last decade in an effort to try to characterize the structure of the metal binding site in proteins, among which Electron Paramagnetic Resonance (EPR) [18], Nuclear Magnetic Resonance (NMR) [19, 20], Circular Dichroism (CD) [18, 20], and XAS [21, 22] are the most prominent ones.

In particular, the availability of a new generation of synchrotron radiation sources has greatly enlarged the range of applications of XAS in the investigation of structural properties of biological systems. Reliable data for a wide range of absorbing atoms, even if very diluted (as it is frequently the case in biological samples), are now accessible. Indeed, XAS can be successfully used to study the environment of metal ions complexed with proteins and peptides in their physiological environment, owing to its chemical selectivity and sensitivity to the local atomic environment around the absorber. An accurate analysis of the extended X-ray absorption fine structure (EXAFS) region of the spectrum in

terms of single plus multiple scattering (MS) events allows a clear-cut identification of the amino acid (a.a.) residues primarily bound to the metal. A well-known example of application of this technique is to metal-enzymes, where the metal either acts as a catalytic center or plays a structural rôle in maintaining the protein active conformation [23-27].

As for the theoretical interpretation of the large body of available experimental data, routine techniques used to model atomic interactions (like Monte Carlo and Molecular Dynamics simulations, Quantum chemistry calculations), though yet limited by the insufficient accuracy of present computational methods, are increasing their capability of investigating the supra-molecular level. Indeed, advances in algorithm development, software implementation and computer hardware are rapidly improving the situation in a promising way.

Understanding the peculiar electronic properties of metal complexes is a necessary step to clarify the role played by metal ions in biochemical reactions. This means that the electronic structure of the compound need to be described at the quantum level, *i.e.* in the framework of the density functional theory (DFT) [28-30] with the special adaptations necessary to cope with applications to bio-molecules. In particular, when dealing with delocalized systems like organo-metallic molecules *ab initio* molecular dynamics simulations of the Car-Parrinello (CP) type [31, 32] are especially well suited.

2.1. X-ray Absorption Spectroscopy

From the experimental point of view, this review will be focused on the XAS technique, as the latter displays a number of very interesting features when it is employed in investigating biological systems, and especially in the study of metal-proteins [27, 33-37]. Perhaps the most important of them is that XAS can be used for samples in any state of aggregation. A further advantage with respect to other spectroscopic techniques is that there are no selection rules that would extinct the signal in unlucky circumstances, with the result that a XAS signal is always non-vanishing. Finally XAS is very sensitive to the nature of the metal absorber. It allows extracting structural information about the absorber atomic environment through the study of the oscillations of the absorption coefficient

originating from the interference between the outgoing electron wave, kicked-off from the metal, and the back-scattered waves emerging from the surrounding atoms (see Appendix A). This interference spectrum contains detailed information about scatterer-absorber relative positions, from which the geometrical and structural arrangement of the a.a.'s that are coordinated to the metal can be inferred with fairly good accuracy. Data analysis requires a rather sophisticated theory, where single and multiple scattering contributions [38, 39] have to be taken into account. For a pictorial description of the behaviour of the electron wave function and the corresponding measured XAS signal see Fig. **1** in [40] in the case of an isolated atomic absorber (left panel), and in the case of an absorber surrounded by other atoms acting as scattering centers (right panel).

2.1.1. Generalities

XAS uses Synchrotron Radiation as source of photons. We recall that for an absorption process the following very general law holds

$$I(E) = I_0 e^{-\mu(E)d} \quad , \qquad \textbf{(1)}$$

where $E = h\nu$ is the energy of the incident photon, $I(E)$ is the intensity of the transmitted radiation, I_0 is the intensity of the incident radiation, $\mu(E)$ is the absorption coefficient characteristic of the system in consideration and d is the thickness of the sample traversed by the photons (see Appendix A for other definitions and more details).

The behaviour of the absorption coefficient, $\mu(E)$, with the photon energy is monotonically decreasing except where the photon energy corresponds to the photo-ionization energy, E_0, of an inner electron of the absorbing atom. Around this energy the absorption coefficient rapidly increases and, if the absorbing atom is isolated (for example when a mono-atomic gas is considered), it starts decreasing soon after the edge energy (see the left panel of Fig. **1** in [40]).

The ionization energy of an inner electron is usually referred to as the "edge energy", or simply the "edge". The K-edge corresponds to the ionization of one of the innermost electrons, while the L-edges correspond to the ionization of the electrons belonging to the next shell, and so on.

At a sufficiently high atomic number the edge energies of the various atoms are well separated, so that the absorbing spectrum of a complex system shows characteristic and well separated peaks. Just to give an idea, the K-edges of Fe, Cu and Zn are located at 7112, 8979 and 9659 eV, respectively. This is the reason that makes XAS such a highly selective technique and allows getting detailed local structural information around a selected atomic absorber.

In a multi-atomic system the value of the absorption coefficient does not decrease monotonically after the edge, as it does for an isolated atom, but it has an oscillating behaviour. As we recalled above (see right panel of Fig. **1** in [40]), the physical explanation for the oscillating behaviour of $\mu(E)$ has its roots in the quantum interference phenomenon. To a very good approximation the wave function of the ionized electron (*photo-electron* in the following) can be described as an outgoing spherical wave centered on the absorber. The atoms surrounding it act as diffusion centers (scatterers) for the impinging wave. In turn the back-scattered waves from the atoms around the absorber interfere with the outgoing spherical wave of the photo-electron, giving rise to the interference phenomenon observed at the absorber location, where the photo-electron wave function is mostly concentrated. The interference will result in a modulation of the modulus square of the total amplitude of the wave function of the photo-electron. As a result the probability of the photon to be absorbed shows maxima or minima, according to whether the outgoing and scattered waves are *in phase* or *out of phase*. Amplitudes and phases of undulations depend on the kind and relative position of absorber and scatterers or, in other words, on the chemical and structural (three-dimensional) arrangement of the absorber atomic environment. This is the same as saying that the interference signal contains information about the local geometrical structure around the absorber.

2.1.2. Analyzing the XAS Spectrum

The XAS spectrum is commonly separated into two energy regions

1. XANES (X-ray Absorption Near Edge Structure) region starting a few eV before the edge energy, E_0, and extending some few tenths of eV above it;

2. EXAFS (Extended X-ray Absorption Fine Structure) region following the XANES region and extending some few hundreds eV above the edge.

3. The XANES region is dominated by a variety of very complicated low energy transfer events. Although this part of the spectrum in principle contains many detailed information about the local atomic structure around the absorber, its theoretical analysis is still at a semi-qualitative level [see, however, the works of refs. [38, 41-44] and limited to cases where quite a precise knowledge about the geometrical arrangement around the absorber is available [45-47].

4. The kinetic energy, $E = h\nu - E_0$, of the photo-electron in the EXAFS region is definitely larger than in the XANES region. At these comparably higher energies, single scattering events are dominant, although MS contributions, that are richer in structural information, are still present and must be taken into account for an accurate analysis of experimental data.

Theoretical approaches [38, 48] giving a rigorous quantum mechanical description of the EXAFS signal, including both single and multiple scattering terms, have been implemented in a number of packages among which we may mention gnXAS [49], FEFF [50] and EXCURV [51, 52] (for a comprehensive review see ref. [53]).

The inclusion of MS terms in the analysis of XAS data is especially important in investigating the structure of the active site in a metal-protein. Amino acidic residues are, in fact, almost completely made of "light" atoms (*i.e.* nitrogen, oxygen and carbon) and their contributions to the total XAS signal are indistinguishable from one another, if the analysis is performed in the single scattering approximation.

Including MS contributions removes to a large extent this limitation. The magnitude of the contributions coming from the presence of a.a.'s around the metal absorber, in fact, turns out to depend not only on the kind and mean

distance of the atomic scatterers, but also on the specific geometrical arrangement of the a.a. lateral chain. A well-known and biologically very important example of this situation is represented by the case of the Histidine (His). The presence of this residue bound to a metal can be fairly well identified in a XAS spectrum because the contribution it gives rise to the signal through MS events is strongly enhanced, owing to the positive interference of amplitudes (focusing effect) resulting from the quasi-collinearity of the atoms belonging to the His imidazole ring with the absorbing atom[1] [54].

2.2. *Ab initio* Simulations

A rigorous and reliable understanding of spectroscopic data can only come from a Quantum Mechanical (QM) approach. In this respect *ab initio* simulations - in particular of the CP type - can be used to extract structural information and discriminate among different models thanks to the detailed atomic knowledge that numerical methods can provide. In this review we will briefly outline the theoretical foundations of such *ab initio* methods (see also Appendix B) and discuss some applications to the case of Aβ-peptide in interaction with metals.

2.2.1. Generalities

The program of *ab initio* simulations is conceptually rather simple but epistemologically very ambitious. In a nutshell it consists in the idea of deriving and studying the physico-chemical (or more modestly the structural) properties of a system starting solely from the knowledge of the fundamental interactions among its elementary constituents (atoms). The beauty and the strength of this approach is that in principle there will be no free parameters to play with, as everything will be finally expressed in terms of fundamental physical constants. The price to pay is the enormously large number of degrees of freedom that should be taken into account in the simulation to get a realistic description of the system, especially if, as it is the case of interest here, one is dealing with biological systems. The necessarily limited computer resources available at any time puts severe bounds to the size (hence to the nature) of the systems that can be attacked and studied in this way. Despite these undeniable difficulties, the recent

[1] A remarkable example of this situation is represented by the interplay between the structure of the active site in a metal-protein and its functionality as discussed, for instance, in ref. [27].

enormous advances in computer design and algorithm development have made this kind of *first principle* approach a really viable and useful computational tool [55].

Indeed, taking inspiration from the general ideas and concepts of Statistical Mechanics, many powerful techniques ranging from deterministic Molecular Dynamics (MD) simulations to stochastic Monte Carlo (MC) and Hybrid MC methods have been set up and numerically implemented [56]. The success of this computational strategy is so big that today one can hope to push simulations into the realm of some of the most difficult, still open biophysical problems, like immunological recognition, drug design or protein folding.

A crucial issue in this field is to decide whether one can deal with classical Newtonian Mechanics and potential theory or whether instead a QM approach is necessary. The nature of the problem one wants to tackle dictates the answer to this question. Simple considerations show that, given the values of pressure and temperature which are of interest in biology, it is perfectly well appropriate to treat atoms as classical particles, provided the potential in which they move is computed at the QM level, *i.e.* by solving the Schrödinger equation for the (outermost) electrons of the atoms which make up the system under study.

The CP method [31] couples in a very elegant and computationally efficient way the classical equations that describe the motion of the atoms of the system to the Schrödinger equation for the associated electrons, with the electrons in turn determining the force field experienced by atoms. In other words, the atoms move classically in the QM potential self-consistently generated by the electrons (see Appendix B). MD simulations of this kind are inherently based on the adiabatic decoupling between atomic and electronic degrees of freedom (*i.e.* on the so-called Born-Oppenheimer approximation). This separation is justified by the observation that the characteristic frequencies of the atomic motion are much smaller (by a factor ~ 10^3) than the typical electronic frequencies.

2.2.2. Car-Parrinello Molecular Dynamics

Car-Parrinello molecular dynamics (CP-MD) simulations for complex systems have been largely and very successfully used in many research areas ranging from

solid-state physics to biological systems. Among the numerous papers in these areas see, for instance, those quoted in refs. [57] and [58], respectively. In applications to the study of metal-protein complexes CP-MD was employed and validated in a detailed structural investigation of the Cu binding sites located in the unfolded PrP octarepeat region [59, 60].

The use of QM methods (as opposed to purely classical MD approaches) for computing the force field felt by atoms is dramatically needed in the study of metal-protein complexes for two reasons. One is of a technical nature and has to do with the presence of a (doubly charged) metal ion in the system, which makes much safer the use of *first principle* simulations, for they embody charge polarization and screening, rather than that of classical MD which would require employing one of the rather sophisticated, but still not fully satisfactory, algorithmic tricks that have been developed to deal with the situation where the long range Coulomb interactions are present [61]. The second reason is more fundamental and it is related to the fact that it is the main purpose of all structural studies to identify the nature of metal ligands. This is of course something that is not known *a priori* and should be the main outcome of the investigation rather than an input as would be the case if one decides to employ classical atomic force fields.

An obvious limitation to the use of QM numerical simulations is the foreseeable very short length of the CP-MD trajectories (few picoseconds - 1 ps $=10^{-12}$ secs) for systems of the size one is interested in in biology, that certainly can never be as extended as one would like it to be. A possible way to cope, at least partially, with the difficulties related to the conflict between the need to deal with a realistically large system and the consequent limitation concerning the length of the simulated trajectory could be to exploit the possibilities offered by the recently developed mixed classical/quantum mechanical methods, like Quantum Mechanics/Molecular Mechanics (QM/MM) [62].

In any case there are good reasons (supported by quite a long experience in the field of CP-MD simulations) that make one to believe that already a few ps trajectory can give useful information on structural problems like those we are interested in this review (*i.e.* identification of primary metal ligands). The argument is based on the observation that CP-MD simulations can be thought of as a way of successively

computing the electronic density while atoms move around. From this perspective CP-MD may be considered not so terribly different from genuine DFT or quantum chemistry computations [28-30], provided one could live with the two well-known problems of the CP-MD method. Namely, the fact that excited electronic states are essentially inaccessible and that atoms will only be able to explore a region of the phase space not too distant from their initial configuration.

It is interesting to note that the application of CP-MD methods to the study of metal-proteins is not set back by any of these two limitations. In fact, what one wants to identify and compare are the coordination modes of different ions (mostly copper and zinc) when complexed with various kinds of amyloid peptides. Indeed, we are only concerned here in understanding what could be the specific rôle of metals just in the very first steps of a possible aggregation process, where statistical equilibrium is not yet an issue. This more modest approach is still of great relevance because it looks that only the compounds that are formed in the very early stage of the aggregation process are pathological. The subsequent steps of mesoscopic fibril formation may on the contrary have a protective effect against neurodegenerative processes [63-65]. In any case fibril formation is driven by an extremely complicated dynamics that at the moment is beyond any possible atomistic description.

A parallel version of the freely-available Quantum-ESPRESSO package (opEn-Source Package for Research in Electronic Structure, Simulation, and Optimization [32, 66]) was used for most of the *ab initio* CP-MD simulations discussed in this review.

To minimize finite volume effects periodic boundary conditions are routinely imposed to the system. The simulated peptide is inserted in a super-cell (filled with water molecules at 1 gr/cm^3 density) with sufficiently large linear dimensions to ensure replicas to have negligible spurious self-interactions. For neutral systems a separation of 4.5-5 Å is considered to be sufficient. For charged systems a separation of at least 8 Å is required.

CP-MD calculations are often performed ignoring the electron spin degree of freedom, *i.e.* in the so-called spin-restricted conditions. This approximation is adequate for the kind of systems we are interested in here.

Before moving to the presentation of the results that have been obtained, it is convenient to provide a few more general information about the CP-MD simulation strategy.

A key issue in CP-MD is the structure of the atomic configuration that is used to start the simulation. Given the effectively rather short time duration of any CP trajectory, it is, in fact, mandatory to start from a very accurately equilibrated and thermalized configuration to avoid biases and instabilities. Usually good initial configurations are those coming from crystallographic or NMR data. If no such structural data are available, one must very carefully prepare the system performing preliminary adequately long (of the order of a few nanoseconds (1 ns = 10^{-9} secs)) classical MD simulations. For this purpose any of the currently available MD codes (like GROMACS [67], Amber [68], *etc.*) can be equally well employed.

At this point the CP-MD procedure can be started. According to a well-established experience, which was thoroughly tested in the works of refs. [59, 60], one has to begin by minimizing again stresses and strains among atoms while electrons are pushed to vanishing "temperature". In summary the CP-MD simulations must be carried out according to the general protocol outlined below.

1. Minimization of electronic energy with fixed atomic positions.

2. Minimization of total energy as a function of both atomic and electronic degrees of freedom of the system.

3. A few short preliminary sequential CP-MD simulations at increasing (say, in step of 50 K or 100K) atomic temperatures up to 300 K, using a Nosé-Hoover thermostat [69] coupled to the atomic degrees of freedom, and kept at the desired temperature.

4. Final CP-MD simulations of appropriate length at an atomic temperature of 300 K with the use of the same thermostat as in 3.

Thermalization in step 3. is necessary to slowly attain room temperature, thus avoiding that temperature oscillations affect in an uncontrolled way the approach

of electrons to their ground state. The velocity Verl*et al*gorithm [70] for integrating the CP equations of motion is most commonly used.

The key question at this point is how long the simulated CP-MD trajectories can be. The answer depends obviously on the size of the system (*i.e.* volume, number of atoms, N_A, and number of electrons, N_e) and the CPU power of the available machines. A careful analysis of the dynamics underlying CP-MD [71, 72] reveals that an acceptable time step for the atomic dynamics and the iterative solution of Kohn and Sham (KS) [29] equations for the electrons (see Appendix B) turns out to be extremely small, namely of the order of 0.10-0.15 femptoseconds (1 fs = 10^{-15} secs). Thus one immediately comes to the conclusion that, at the moment, it is very hard to get trajectories longer than ~ 10 ps for the kind of systems we are discussing in this review, where a few 10^2 atoms and up to 10^3 electrons are involved.

3. Aβ-Peptides

In this section we present and discuss the results of the extensive study[2] carried out on a set of selected fragments of the Aβ-peptide complexed with either Cu^{2+} or Zn^{2+} [74].

3.1. XAS Experiments

The particular fragments that have been considered in [74] are listed in Table **1**. They have been selected for a number of different reasons. $A\beta_{1\text{-}16}$ is the minimal fragment which contains the three His's (His_6, His_{13} and His_{14}) that have been identified as metal ligands [18, 20], while $A\beta_{17\text{-}40}$ is the complementary sequence where none of these His's is present. In the $A\beta_{1\text{-}28}$ fragment a long hydrophobic region, believed to be relevant in the aggregation processes, is also contained. Finally the $A\beta_{5\text{-}23}$ fragment was measured with the main purpose of trying to answer the question on whether or not the N-terminal region of the Aβ-peptide in involved in the metal binding process.

Besides confirming the general results of [22] concerning the existence of important structural differences between Cu^{2+} and Zn^{2+} coordination modes, XAS

[2] All the XAS data presented in this section have been collected at the D2 bending magnet beam line of the EMBL Outstation Hamburg at DESY [73]. The X-ray spectra of the samples were recorded in fluorescence mode.

experiments have been able to elucidate the special rôle played by the N-terminal region in binding the metal. In particular, it was found that only two His residues remain coordinated to Cu^{2+} when the first four a.a. residues are cut out (as is the case in the Cu-$A\beta_{5-23}$ sample). The natural explanation for this peculiar feature is that, among the three His residues (His_6, His_{13} and His_{14}) generally relevant in metal coordination, it is His_6 that is no more available for Cu binding, because binding with the latter is now hindered by the proximity of the dissociated N-terminus.

The situation with Zn-Aβ complexes is somewhat different. It is, in fact, observed that cutting out the first four a.a. residues of the peptide does not modify the number of coordinated His's, as was the case of Cu complexes. The spectrum in the EXAFS region remains unaltered and XAS results are in all cases compatible with four coordinated His's, indicating that each metal ion is shared by two Aβ-peptides. The absence of the first four a.a. residues only affects the local geometry around the Zn absorber, as it is demonstrated by the, instead, markedly different structure of the XANES region of the spectrum of the Zn-$A\beta_{5-23}$ sample with respect to that of all the others.

Table 1: The amino acidic sequence of the five Aβ oligopeptides under consideration.

Oligopeptide	**a.a. Sequence**
$A\beta_{1-16}$	H_3N^+-DAEFRHDSGYEVHHQK-COO^-
$A\beta_{1-28}$	H_3N^+-DAEFRHDSGYEVHHQKLVFFAEDVGSNK-COO^-
$A\beta_{5-23}$	H_3N^+-RHDSGYEVHHQKLVFFAED-$COOH_3N^+$
$A\beta_{17-40}$	H_3N^+-LVFFAEDVGSNKGAIIGLMVGGVV-COO^-
$A\beta_{1-40}$	H_3N^+-DAEFRHDSGYEVHHQKLVFFAEDVGSNKGAIIGLMVGGVV-COO^-

3.1.1. Data Analysis

As we mentioned at the beginning of sect. 2.1.2, XAS spectra are normally analyzed by separating out the XANES region of the spectrum, from the EXAFS region that extends from about a few tens of eV's beyond the edge onward. In fact, the difficulty of getting a reliable theoretical description of the very complicated electronic processes affecting the low-energy part of the spectrum makes its quantitative interpretation very problematic [38, 41-44]. At the same time,

however, the structure of this small slice of the spectrum is very sensitive to the electronic structure of the absorber and the symmetry of the local environment around it, and can yield valuable information on similarities and differences when relative local geometries of structurally similar samples are compared [33]. At variance with this situation, valuable quantitative structural information can be more easily extracted from the EXAFS region, even starting with limited a priori knowledge on the atomic structural environment around the absorbing metal. For these reasons in this review we will limit the discussion to the EXAFS region of the measured spectra.

From a general comparison of the EXAFS portions of the spectra of the 10 samples (*i.e.* five Aβ fragments complexed with either Cu or Zn) that have been subjected to XAS measurements reported in ref. [74], an interesting pattern of strong similarities and differences emerge that are summarized below where the equality sign means identity (within errors) of spectral features (see Figs. (**2**) and (**3**) in [40]).

- (Dis-)similarities among EXAFS spectra of Cu complexes

$$\text{Cu-A}\beta_{1\text{-}16} = \text{Cu-A}\beta_{1\text{-}28} = \text{Cu-A}\beta_{1\text{-}40} \neq \text{Cu-A}\beta_{5\text{-}23} \neq \text{Cu-A}\beta_{17\text{-}40}$$

- (Dis-)similarities among EXAFS spectra of Zn complexes

$$\text{Zn-A}\beta_{1\text{-}16} = \text{Zn-A}\beta_{1\text{-}28} = \text{Zn-A}\beta_{1\text{-}40} = \text{Zn-A}\beta_{5\text{-}23} \neq \text{Zn-A}\beta_{17\text{-}40}$$

On the basis of the previous comparison, discussion and fitting of the data have been limited to the following samples

1. Cu-A$\beta_{1\text{-}16}$, as a prototype of Cu-A$\beta_{1\text{-}16}$, Cu-A$\beta_{1\text{-}28}$ and Cu-A$\beta_{1\text{-}40}$ samples.

2. Cu-A$\beta_{5\text{-}23}$, as its EXAFS spectrum is different from that of Cu samples above.

3. Zn-A$\beta_{1\text{-}16}$, as a prototype of Zn-A$\beta_{1\text{-}16}$, Zn-A$\beta_{1\text{-}28}$, Zn-A$\beta_{1\text{-}40}$ and Zn-A$\beta_{5\text{-}23}$ samples.

No fitting of the Cu-Aβ_{17-40} and Zn-Aβ_{17-40} data was carried out because the EXAFS spectra of these samples are identical to those of Cu and Zn in their respective buffers ($CuSO_4$ and $ZnCl_2$). This spectral equality is simply interpreted as a signal of the fact that the Aβ_{17-40} fragments are not able to bind the metal[3].

3.1.2. EXAFS Results

EXAFS data have been analyzed and fitted employing the EXCURV98 package [52]. The procedure implemented in the code is essentially fully automated except for the crucial question of how to choose the initial configuration that should be used to start the fitting algorithm. Concerning this point, as recommended in the literature [19, 20, 22, 75, 76], the strategy that was followed in ref. [74] was to try out various initial geometrical models, differing in the number of His's involved in the metal coordination, with structures taken among the many collected in the Metalloprotein Database and Browser (MDB) [77].

Best fit parameters are listed in Table **2**[4]. It should be remarked that the distance, *r*, reported there, refers to the position of either the coordinated atom or the "leading" atom of the corresponding a.a. residue. By "leading" atom of His (or Tyrosin, Tyr) we mean the N-imidazole (or the O-hydroxyl) atom through which the residue is bound to the absorber. It is important to note here that, even if in general it is not possible to distinguish among light scatterers (like N, O and C) only on the basis of their individual contribution to the EXAFS signal, when acting as leading atoms, they can be generally identified in a unambiguous way because they are tightly anchored to a large and well ordered bunch of other atoms.

Oxygen atoms, that are simply indicated by O in Table **2**, belong to a water molecule or to a.a.'s other than His or Tyr. As for the quality of the fits, we see that in all cases experimental data are rather well reproduced with values of the *r*, *N* and σ_{DW} parameters that are fairly accurate and physically very reasonable. This consistency pattern is confirmed by the nice correspondence between the location and the height of the peaks of the FT of experimental and theoretical signals.

---

[3] It should be remarked that the harmless α- and γ-secretases cleavage of APP precisely cuts out the first 16 a.a.'s of Aβ-peptide.

[4] Experimental and theoretical spectra are shown in Figs. (**4**), (**5**) and (**6**) of Ref. [40].There the left panel of show the fitted (black line) and experimental (grey line) spectrum of the Cu-Aβ_{1-16}, Cu-Aβ_{5-23}, and Zn-Aβ_{1-16} samples. The modulus of the Fourier Transform (FT) of both the experimental and theoretical spectrum is reported in the right panel.

Table 2: Best fit parameters characterizing the atomic arrangement around the absorber in the Cu-$A\beta_{1-16}$, Cu-$A\beta_{5-23}$ and Zn-$A\beta_{1-16}$ samples. First and second columns show type and number, *N*, of coordinated chemical groups (atom or residue). Third and fourth column show distance, *r*, from the absorber of the coordinated atom or the leading atom of the coordinated residue and corresponding value of Debye-Waller (DW) factors, σ^2. Errors are only statistical. In the last row we report for each sample the Fermi energy shift, ΔE_F, and the fit quality factor, *R*.

Coord. Residue/Atom	***N***	$r \pm \Delta r$ Å	$\sigma^2 \pm \Delta\sigma^2$ Å^2
Cu-$A\beta_{1-16}$			
His	3	1.95 ± 0.01	0.002 ± 0.001
Tyr	1	2.06 ± 0.01	0.002 ± 0.001
O	1	1.95 ± 0.01	0.002 ± 0.001
ΔE_F = -10.2 ± 0.7 eV R = 28%			
Cu-$A\beta_{5-23}$			
His	2	1.99 ± 0.01	0.003 ± 0.001
Tyr	1	1.99 ± 0.01	0.003 ± 0.001
N (terminus)	1	1.99 ± 0.01	0.003 ± 0.001
O	1	2.27 ± 0.01	0.003 ± 0.001
ΔE_F = -13.8 ± 0.4 eV R = 40%			
Zn-$A\beta_{1-16}$			
His	2	1.96 ± 0.01	0.003 ± 0.001
His	2	2.00 ± 0.01	0.003 ± 0.001
O	1	2.00 ± 0.01	0.003 ± 0.001
ΔE_F = -6.5 ± 0.2 eV R = 23%			

Cu complexes - The best fit for the Cu-$A\beta_{1-16}$ sample corresponds to a site configuration in which three His's and one Tyr are included in the Cu coordination sphere, plus an oxygen possibly belonging to a water molecule or to an a.a. other than His or Tyr. This structure is the one already proposed in [22] for the Cu-$A\beta_{1-40}$ peptide. However, it should be pointed out that in the case of the Cu-$A\beta_{1-16}$ complex the model, in which the Tyr oxygen is replaced by the nitrogen of the N-terminus, gives rise to a fit only marginally worse than the one whose structural parameters are reported in Table **2**. Consequently one cannot completely rule out the possibility of a Cu coordination with the N-terminal nitrogen replacing the Tyr residue.

The situation one encounters here is an important example of a case where *ab initio* simulations can be of help in answering the question whether it is the Tyr

oxygen or the N-terminal nitrogen which is coordinated to Cu. We will take back this point in sect. 3.2.

Moving now to the Cu-Aβ_{5-23} sample, one realizes that a satisfactory fit cannot be obtained if the coordinated residues are the same as for Cu-Aβ_{1-16} and only their geometrical parameters are left free to move. A good fit is instead found starting from a configuration, inspired by the work of ref. [78], in which His_6 is replaced by the N-terminal amino group. In this model Cu^{2+} is coordinated to two His's, one Tyr, the nitrogen belonging to the N-terminal amino group, and one oxygen. The fact that, by cutting out the first four a.a.'s, the number of coordinated His's is reduced from three to two, is a strong indication that His_6 is the third residue normally bound to the metal. The loss of the His_6-metal bond is to be ascribed to the strains induced by steric hindrance effects when a.a.'s from 1 to 4 are missing.

Zn complexes - Just like in the case of Cu complexes, the Zn-Aβ_{17-40} spectrum is almost identical to that of Zn in buffer. This identity confirms that the absence of the first 16 a.a.'s prevents metal binding. However, at variance with Cu complexes, here it turns out that also the EXAFS spectrum of Zn-Aβ_{5-23} is very similar to the spectrum of the three other Zn-samples (*i.e.* Zn-Aβ_{1-16}, Zn-Aβ_{1-28} and Zn-Aβ_{1-40}) comprising the first four a.a.'s of the Aβ-peptide sequence. Then, as a prototype of the above four (almost) identical Zn complex spectra, only Zn-Aβ_{1-16} EXAFS data were considered and subjected to a quantitative analysis. The best fit to the data is obtained by including in the Zn coordination sphere four His's and one oxygen. This structure is of particular relevance and it is perhaps one of the most interesting results obtained in these experiments. Recalling, in fact, that each Aβ-peptide at most contains three His's, this finding means that in order for the metal to be coordinated to four His's, at least two different peptides must be involved in the Zn binding mode.

This conclusion should be considered an extremely important result which points in the direction of a propensity of Zn (at variance with Cu) to form a sort of a network of Aβ-peptides with the metal stabilizing the whole structure by binding His's belonging to adjacent peptides (see also [79]). In the next section we will see that these conclusions are nicely confirmed by *ab initio* simulation results.

3.2. CP-MD

In this part of the review we want to discuss how *ab initio* simulations (in particular CP-MD simulations) can be used to interpret experimental results and possibly discriminate among different models owing to the detailed atomic information that numerical methods can provide[5].

In the following sections we want to show how to set up an effective strategy to investigate, in the important instance of Aβ-peptides, the rôle played by metallic ions (specifically Cu and Zn) in giving the protein its functionality or, on the contrary, in transforming it into a pathogenic conformer. For this study the knowledge of the structure of the metal-Aβ binding site is a key prerequisite.

3.2.1. Cu-Aβ-Peptides

We start to discuss the case of Cu. The experimental situation is not completely satisfactory here as there are in the literature somewhat conflicting results about the Cu coordination mode in Aβ-peptides. On the one hand, in fact, NMR data on Cu complexed with $A\beta_{1\text{-}28}$ [18] and $A\beta_{1\text{-}40}$ [76] peptides suggest that three His's (His_6, His_{13} and His_{14}) are coordinated to the metal with the fourth ligand being a nitrogen from the N-terminus. On the other, XAS experiments on various portions of the $A\beta_{1\text{-}40}$ peptide [22, 74] and NMR/EPR experiments on the $A\beta_{1\text{-}28}$ peptide [82], as well as NMR data on the $A\beta_{1\text{-}16}$ [20] fragment, all point to the conclusion that, besides the above three His's, the fourth Cu ligand is the Tyr_{10} oxygen.

In these circumstances a natural application of the CP-MD theoretical approach is thus to compare the two structural situations where, besides His_6, His_{13} and His_{14}, either the N-terminus or the Tyr_{10} oxygen is coordinated to Cu, with the aim of determining which one of the two atomic arrangements is the physically realized one. This is done by studying the stability properties of the two configurations along the simulated CP-MD trajectories.

We stress that clarifying this point is not without interest, as it is expected that the more or less open structure of the peptide can strongly influence its aggregation

[5]Although a QM approach is the method of choice for this kind of problems, we wish to mention that there have been interesting classical MD simulations of stacks of β-amyloid peptides (in the absence of metals) confirming experimental indications [80] about the peculiar way in which in their early stage of aggregation peptides may be packed and structured [81].

propensity. One may suspect that a coordination mode where the N-terminus is not bound to Cu will typically give rise to a more open geometry, which would probably be more prone to aggregation.

3.2.1.1. Models Construction

In order to tackle the structural problem described above three specific Cu-Aβ complex model systems (denoted by S_1-Cu, S_2-Cu and S_3-Cu in the following and described below) have been set up for CP-MD simulations [83]. For reasons we have already explained, their detailed atomic structure is constrained by a compromise between the need of having a sufficiently realistic description of the actual physical system and the impossibility of dealing with too many atoms and electrons. According to this criterion the simulated model systems have been built up as follows. First of all, attention was limited to the $A\beta_{1-14}$ segment (see Table **1**) where the Cu binding site is known to be located. Secondly, since the His_6, His_{13} and His_{14} residues have been positively identified as Cu ligands, they are all explicitly included with the full atomic structure of their lateral chains. As for the other a.a.'s, somewhat different choices for the S_1-Cu, S_2-Cu and S_3-Cu systems (see below) are considered. In all cases the C-terminus is capped in the usual way (*i.e.* by an $NHCH_3$ group), while the N-terminus of the fragment is left open (with an ending NH_2 group) to allow for possible Cu binding accompanied by the loss of the amine hydrogen. Periodic boundary conditions are used and the size of the box was chosen in such a way that the distance between any atom and its nearest image is at least 5 Å. The whole system is neutral as the double positive charge of Cu^{+2} is balanced by the sum of the negative charges of Asp_1 and Glu_3. The detailed structures of the three model systems are described here below and sketched in Fig. **1**.

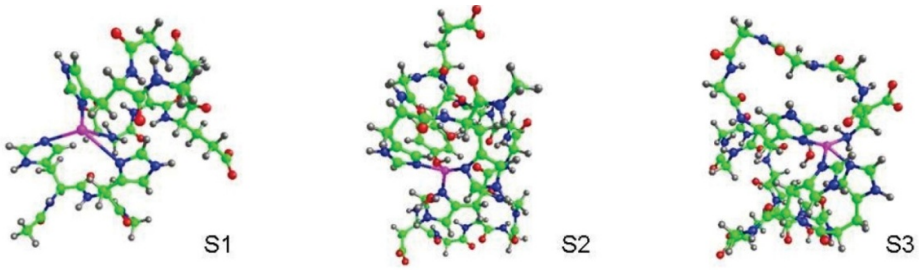

Figure 1: The atomic structure of the S_1-Cu, S_2-Cu and S_3-Cu model systems (denoted S_1, S_2 and S_3 in the figure). Colors are as follows: gray is H, red is O, green is C, blue is N, and magenta is Cu.

• S_1-Cu System

Of the first six a.a.'s (from 1 to 6), besides the backbone, only the lateral chains of Asp_1, Glu_3, and His_6 are retained. Among the remaining a.a.'s (from 7 to 14) only His_{13} and His_{14} with their lateral chains are explicitly included. The His_{13}-His_{14} dipeptide is capped with a CH_3CO group at its N-terminus and by an $NHCH_3$ group at its C-terminus. The system, solvated with 125 water molecules, is contained in a box of volume V=14×19×19 $Å^3$. In this way density is equal to 1 g/cm_3. All in all, the system (including Cu and water molecules) is made by 494 atoms. The number of KS (see Appendix B) electrons (*i.e.* the electrons that are considered relevant in determining the inter-atomic potential) is 1369. The initial peptide configuration for the CP-MD simulations was taken from the PBD file of [75] with Cu replacing Zn.

• S_2-Cu System

The backbone of the whole 1-14 peptide is retained together with the full lateral chains of Asp_1, His_6, Tyr_{10}, Glu_{11}, His_{13}, and His_{14}. The system, solvated with 225 water molecules, is contained in a box of volume V=22×23×20 $Å^3$. In this way density is equal to 1 g/cm^3. All in all, the total number of atoms of the system (including Cu and water molecules) is 838 and the number of KS electrons is 2311. The initial configuration for the CP-MD simulations has been taken from a 8 ns long classical MD simulation of the whole Cu-$A\beta_{1-16}$ peptide in water with His_6, His_{13}, His_{14} and Tyr_{10} bound to Cu. For this step the GROMACS package [67] was used.

• S_3-Cu System

The backbone of the whole 1-14 peptide is retained together with the lateral chains of Asp_1, His_6, Tyr_{10}, Glu_{11}, His_{13}, and His_{14}. The system, solvated with 223 water molecules, is contained in a box of volume V=20×24×20 $Å^3$. In this way density is equal to 1 g/cm^3. All in all, the total number of atoms of the system (including Cu and water molecules) is 832, and the number of KS electrons is 2295. The initial configuration for the CP-MD simulations has been taken from a 6 ns long classical MD simulation of the whole Cu-$A\beta_{1-16}$ peptide in water with His_6, His_{13}, His_{14} and the N-terminus bound to Cu. For this step the GROMACS package [67] was used.

Comparing the various model systems, we observe that the S_1-Cu model is a rather crude approximation of the Cu-A$\beta_{1\text{-}14}$ peptide. The S_2-Cu and S_3-Cu models are more realistic and differ only for the fact that besides His_6, His_{13}, His_{14}, in the case of S_2-Cu the fourth Cu ligand is Tyr_{10}, while in the case of S_3-Cu the fourth ligand is the N-terminus. In all cases a water molecule is present in the Cu coordination sphere as a fifth ligand.

3.2.1.2. Results

• S_1-Cu System

Starting from the atomic configuration suggested by the NMR experiments of ref. [75], a thermalization step consisting of two simulations of 0.6 ps at 100 and 200 K was first carried out. After that, a CP-MD trajectory of 1.4 ps at room temperature (300 K) was generated. The main outcome of the simulation is that, starting from a configuration where, besides the imidazole rings of His_6, His_{13} and His_{14}, the nitrogen of the N-terminus was lying inside the Cu coordination sphere, the system ended up in a state where only the three His's remained coordinated to Cu, while the N-terminal nitrogen had moved far out from it[6].

• S_2-Cu and S_3-Cu Systems

The S_1-Cu simulations indicate that the tentative conclusion drawn from the NMR measurements of refs. [18] and [76] according to which the N-terminal nitrogen is one of the Cu ligand, is not tenable. In order to try to reliably identify the structure of the Cu site, simulations of the more realistic systems S_2-Cu and S_3-Cu were carried out with the purpose of comparing the two situations where the oxygen of Tyr_{10} (S_2-Cu) or the N-terminus (S_3-Cu) is coordinated to Cu at the initial step of their respective CP-MD trajectory. The possibility that the Tyr_{10} oxygen is a Cu ligand was suggested in [20] and confirmed in [22, 74], but criticized in [84, 85].

To prepare the systems for the successive *ab initio* calculations, the S_2-Cu and S_3-Cu systems have been first submitted to classical MD simulations in order to obtain well-equilibrated atomic configurations. From these configurations the

[6] This feature is clearly visible when comparing Figs. (**10**) and (**11**) in [40], where as functions of time (for completeness also the history of the initial thermalization steps is reported) the distances from Cu of the nitrogen atoms of the N-terminus and of $N_\delta(His_6)$, $N_\square(His_{13})$ and $N_\delta(His_{14})$ are displayed. From the same figures it is clear that the N-terminal nitrogen moves quickly away from Cu reaching a distance of about 7 Å at the end of the simulation.

long procedure for CP-MD simulations described at the beginning of this Section is started. Already at the end of the two minimization steps (steps 1 and 2 above) some interesting differences between the two systems are visible. Namely, in spite of the fact that at the beginning of the classical MD step the $N_\delta(His_6)$, $N_\varepsilon(His_{13})$, and $N_\delta(His_{14})$ atoms were located at the same positions around Cu in the two systems, at the end of classical MD and after the atomic energy minimization step, quite different geometrical arrangements are reached. In fact, the system S_3-Cu ends up with a characteristic planar geometry around Cu, similar to the one we saw in the case of the S_1-Cu system. This is not so in the case of the S_2-Cu system, where the dihedral angle $N_\delta(His_6)$-Cu-$N_\varepsilon(His_{13})$-$N_\delta(His_{14})$ is always pretty far from 180°.

It is interesting to note that in ref. [86] the structure of the Cu^{2+}-imidazole complex in water was studied by a combined theoretical analysis of EXAFS and XANES data, coming to the conclusion that a square-pyramidal geometry around Cu is preferred (over the planar or octahedral one) and persists through other Cu complexes like $[Cu^{2+}(H_2O)_5]$ and $[Cu^{2+}(NH_3)_4(H_2O)]$ (see refs. [87] and [88]). Remarkably, the *ab initio* simulations of the S_2-Cu model system, besides confirming this conclusion, are able to give us the extra information that the Cu ligands in the Cu-$A\beta_{1\text{-}14}$ complex are the His_6, His_{13}, His_{14} and Tyr_{10} residues, through the N_δ, N_ε, N_δ and O atoms, respectively.

3.2.2. Zn-Aβ-Peptides

The importance of studying Zn-Aβ complexes stems from the observation that Zn is seen to induce Aβ aggregation more effectively than Cu [89, 90]. From a structural point of view, while to date most of the experimental results [19, 91] and numerical simulations [92, 93] converge to the conclusion of a stable intra-molecular Cu coordination, the situation appears to be much more complicated for Zn^{2+}-Aβ-peptide complexes where several Zn^{2+} coordination modes have been proposed [74, 76, 79, 94].

Thus it appears to be of the utmost importance to understand and clarify whether and how Cu^{2+} and Zn^{2+} differ in their way of interacting with amyloidogenic peptides in general, and Aβ-peptides in particular. For Zn, NMR investigations

have suggested a variety of inter- and intra-molecular [19, 75, 76] metal binding modes involving, besides other ligands, different numbers of His's. The existence of a variety of inter-molecular binding modes was put in evidence by XAS studies [21, 22, 74], among which a rather peculiar and somewhat unusual four-His Zn binding mode. It should be stressed, in fact, that over 5854 PDB entries containing at least one Zn only one case is found [95] where Zn is coordinated to four His side-chains belonging to the same protein monomer (PDB code 1PB026). In a second case the four His side-chains coordinated to Zn belong to different monomers (PDB codes 1HWT and 1QP927).

There is another worth mentioning feature of Zn binding to Aβ-peptides that should be stressed. Experimental data suggest that the four involved His's are made by the two pairs of consecutive, His_{13} and His_{14}, residues coming from two adjacent Aβ-peptides. This structure gives rise to a very special arrangement, as structural databases report one single instance where a metal (actually Cu) is bound to two His's that are one next to the other along the protein sequence [96]. There are instead many cases where Cu is coordinated to four His's side-chains belonging to the same monomer, but all of them concern proteins belonging to the wide class of Cu,Zn-superoxide dismutase (Cu,Zn-SOD) proteins. Actually a fully Zn-substituted SOD enzyme (encoded by the human SOD1 gene) has been shown to be at least as stable as the wild-type heterodinuclear protein [97].

The coordination of Zn by four neutral imidazolyl groups is infrequent even within non-protein coordination complexes. A search for this coordination in the Cambridge structural data- base (CSD) [98] yields, with the exception of tetraimidazole Zn^{2+} perchlorate, only structures in which the imidazolyl group is either deprotonated (imidazolate) or N-methyl protected.

One might be tempted to conclude that the peculiar Zn binding mode found in recent experimental data is a hallmark of peptide aggregation. Although XAS data certainly give a significant indication in this direction, their consideration alone is not enough to reach such a conclusion. In fact, it is certainly true that the strength of XAS resides in its sensitivity to short-range order as it allows us to reliably identify at atomic resolution the average structure around the metal absorber for systems in any state of aggregation. But this same feature seems to result in a

significant limitation in this case, where in order to fully understand the complicated peptide aggregation mechanism assisted by metals, one must be able to reconstruct the structure of the system at distances larger than 6 Å from the absorber. It appears, in fact, that *in vivo* rather large oligomeric or polymeric structures get formed.

3.2.2.1. Models Construction

For the purpose of investigating fibril aggregation, it is not enough to "simply" reproduce the Zn-K-edge XAS spectra (for which, as we just said, the knowledge of the atomic geometry in a small sphere of radius, say, 5-6 Å is enough). Rather it is necessary to be able to identify what are the stable Zn-Aβ-peptide organized structures (for which the knowledge of the geometry of the sample at large is required). For this reason one is led to the use a combined two-step strategy (XAS data fitting plus *ab initio* simulations) to pass from local structural geometry to large scale modeling [99].

In order to build a model of the Zn-Aβ-peptide complex compatible with the experimental XAS data, a number of systems were constructed and submitted to simulations. In particular, based on general structural information and more or less sophisticated numerical methods (ranging from empirical modeling of single and multiple peptide compounds to small truncated *first principle* simulations - the latter being dealt with at the level of the density functional theory), four models (S_i-Zn, i=1,2,3,4**)** are constructed and then optimized (*i.e.* fitted) against the available XAS data. The four models are assembled by putting together two identical $A\beta_{1\text{-}16}$ chains (A e B in the following), with the two nitrogen atoms, $N_\delta(His_{14}^{(A)})$ and $N_\delta(His_{14}^{(B)})$, bound to a single Zn. After a first energy minimization, this initial configuration is further relaxed by a Monte Carlo random walk [100] (MCRW) method. The method consists in randomly changing all the dihedral angles of the two peptide chains, with the exception of those belonging to the two His_{14} side chains that were held fixed to keep the $N_\delta(His_{14}^{(A)})$-Zn-$N_\delta(His_{14}^{(B)})$ motif blocked in space. Among the many configurations produced in this way a few of them are retained, those that appear to fulfill the required geometrical and structural constraints. The virtue of the

random walk sampling method is that no configurations of the Zn-bridging dimer with ''bad'' contacts between pairs of atoms are ever accepted.

• S_1-Zn Model

This model corresponds to one particular configuration of MCRW trajectory in which Zn is closer than 3 Å from $N_\varepsilon(His_{13})$ in both monomers. The reason for this choice is that, among the other possible four-fold metal coordinations, the configuration in which Zn is coordinated to $N_\varepsilon(His_{13}{}^{(A)})$, $N_\delta(His_{14}{}^{(A)})$, $N_\varepsilon(His_{13}{}^{(B)})$ and $N_\delta(His_{14}{}^{(B)})$ is, according to NMR data [75] and Car-Parrinello (CP-MD) simulations, [94] the most stable one.

• S_2-Zn Model

Along the MCRW trajectory a configuration is selected where Zn is coordinated to three His imidazole rings in a 3N1O configuration (with the oxygen coming from the main chain of one of the bound His's). This model was built with the purpose of testing whether a three-imidazole Zn geometry can be compatible with the XAS results of ref. [74]. The reason for binding the oxygen of His_{14} is that the resulting geometry mimics a sort of "half-His" structure, in the sense that from the XAS point of view only half of the pathways available to the photo-electron, compared to the situation in which the metal is bound to an imidazole ring, are now allowed.

The Zn-bridged $A\beta_{1\text{-}16}$ dimers of S_1-Zn and S_2-Zn models were truncated down to systems affordable by semi-empirical and *first principle* methods. In particular the segments 1-10 of both peptide chains were removed and the Glu_{11} N-terminal was capped with the usual acetyl group. Since, as also suggested by the analysis of XAS data, Zn is preferably penta-coordinated, the oxygen of a water molecule is brought at a binding distance from the metal as a fifth Zn ligand. Each truncated dimer was merged into an orthorhombic cell whose dimensions were determined in order for the periodic replicas to be separated by 0.5 nm. The cell is filled with 376 TIP3P [101] water molecules.

In order to check for the stability of the Zn coordination, the resulting configurations of the S_1-Zn and S_2-Zn models were finally subjected to a full

quantum-mechanical step using CP-MD [31]. It is a well recognized fact that classically unnoticed instabilities are easily amplified to a visible magnitude by even very short (of the order of a few picoseconds) quantum-mechanical simulations of the CP-MD type [102].

• S_3-Zn Model

A third model was designed, slightly modifying the S_1-Zn model, by substituting the H_ε atom of $His_{14}^{(A)}$ with a second Zn ion. In the following we will refer to the two Zn atoms as Zn_a and Zn_b. The extra Zn_b, coordinated to one nitrogen from the His bridging the two Zn ions and two oxygens from the Glu_{11} side-chain, is added to check whether its presence is able to stabilize the four-His coordination of Zn_a.

• S_4-Zn Model

A final model, intended to represent a hypothetic, perhaps more realistic situation, is obtained by adding a third peptide fragment (chain C, truncated down to a 11-16 fragment, as it was done for chains A and B), with $N_\varepsilon(His_{13}^{(C)})$ and $N_\delta(His_{14}^{(C)})$ in the same positions as the two water molecules that were bound to the second Zn site (Zn_b site) in model S_3-Zn at the end of the CP-MD simulation (see Table **3** below).

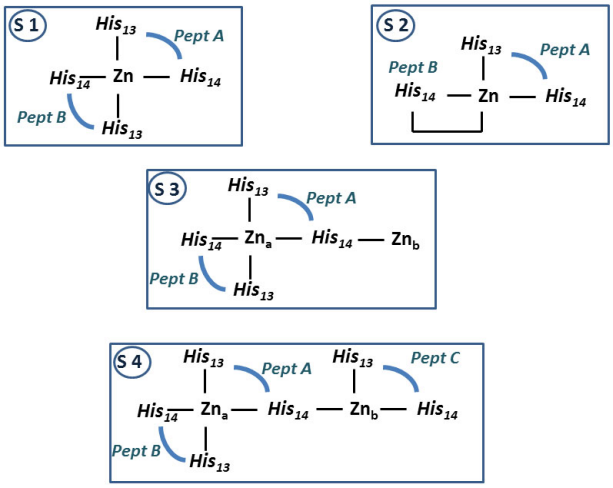

Figure 2: Schematic view of the Zn site in the four models we have constructed. His's connected by blue bands belong to the same peptide. The staple comprising His_{14} and Zn in the S_2-Zn model (in the figure the four S_i-Zn models (i=1,2,3,4) are simply denoted S_i) is there to recall that, besides three imidazoles, the oxygen of the His_{14} main chain is also bound to the metal.

In Fig. **2** for the reader's convenience we sketch the structure of the metal binding site in the four different models we have described. In particular we show which of the the His's are bound to which Zn ion.

3.2.2.2. Results

The relevant features of the evolution of the configurations of the S_i-Zn, i=1,2,3,4 models during the thermalization process are summarized in Table **3**. In the second column of Table **3** (starting configuration) the Zn coordination modes of the four systems before CP-MD (for models S_1-Zn, S_2-Zn and S_3-Zn) or Born-Oppenheimer molecular dynamics (for model S_4-Zn) simulations are listed. Heating the systems from 0 to 250 K (third column), one notices that in both the S_1-Zn and S_2-Zn models Zn loses one ligand and ends up in a tetrahedral 3N1O coordination. For what concerns model S_3-Zn, it is very remarkable that the unlikely initial three-fold coordination of the extra Zn_b readily becomes a more realistic tetra-coordination owing to the oxygen of a water molecule that is attracted within its coordination shell (2.5 Å). Interestingly enough the Zn coordination of both metal sites in model S_4-Zn remains stable along the whole simulation. In the last column, we report the final modifications (when they occur) that take place when the systems are brought to room temperature. We see that the only thing that happens is that in model S_3-Zn one of the two Zn_b-coordinated $O(Glu_{11})$ atoms is replaced by the oxygen of a second water molecule attracted within the coordination shell.

Table 3: For each system in the first column, we report in the second column the atoms that lie within 2.5 Å from Zn (*i.e.* inside the Zn-coordination shell) before the CP-MD or BO-MD simulations. The subscripts (His, Glu, W) denote the residue/molecule to which the atom belongs (W stands for water). In S_3-Zn and S_4 -Zn models the two Zn atoms are denoted Zn_a and Zn_b. In the third and fourth columns the structural variations observed at the end of the simulations at temperatures up to 250 K and at 300 K, respectively, are reported. A''minus'' indicates that a ligand leaves the Zn coordination sphere, while ''plus'' that it enters it.

		Zn-binding modification	
Name	Starting configuration	0–250 K	300 K
S1	Zn: $4N_{His}$ + $1O_W$	$-1N_{His}$	None
S2	Zn: $3N_{His}$ + $1O_{His}$ + $1O_W$	$-1O_{His}$	None
S3	Zn_a: $4N_{His}$ + $1O_W$ Zn_b: $1N_{His}$ + $2O_{Glu}$	Zn_b: $+1O_W$	Zn_b: $-1O_{Glu}$ + $1O_W$
S4	Zn_a: $4N_{His}$ + $1O_W$ Zn_b: $3N_{His}$ + $1O_{Glu}$	None	None

The detailed analysis of the four S_i-Zn models carried out in [99] shows that the S_4-Zn model is not only able to nicely fit the experimental findings of ref. [74], but it remains with the Zn ions in a stable coordination mode all along the numerical simulation steps. The stable geometry of the model is displayed in Fig. **3**. We see that Aβ-peptides are pairwise cross-linked by Zn ions, with one Zn bonded by two pairs of adjacent His's (His_{13} and His_{14}) from two peptides, and a second Zn, replacing the proton in the NH group of one of the involved imidazolyl side-chains, necessary to stabilize the whole system. This pattern can possibly repeat itself thus including a large number of monomers. Indeed, the extensive *first principle* (CP-MD) and semi-empirical (tight-binding methods and Born-Oppenheimer molecular dynamics) combined simulations that have been performed support the picture of a Zn-assisted deprotonation of (at least) one of the His side-chains of the peptide leading to the formation of aggregated complexes.

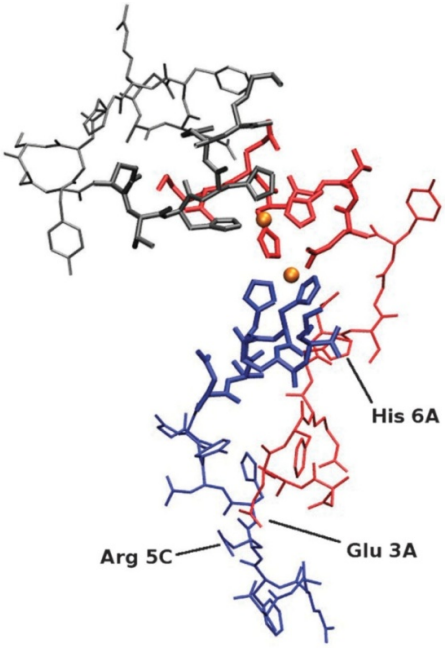

Figure 3: Final MD (t = 500 ps, T = 300 K) configuration of the S_4-Cu model (in which the full $A\beta_{1-16}$ peptide is shown). Zn atoms are displayed in orange, atoms are displayed with sticks, hydrogen atoms are not shown. Chain A is in red, B is in gray and C is in blue. Bonds in the 11-16 residue regions are thicker than those in the 1-10 regions.

4. CONCLUSIONS AND OUTLOOK

Although we are still far from a clear understanding of the rôle of metals in protein misfolding and/or aggregation, experimental and theoretical studies have enormously increased our knowledge in this exploding research area.

In the case of Aβ-peptides experimental information [22, 74] point to a markedly different behaviour depending on whether Cu or Zn is involved in the game. While Cu is bound to Aβ-peptides in rather packed and stable configurations, Zn binding is more flexible and seems to be able to give rise to networks of cross-linked peptides [19].

Detailed *ab initio* studies of the mechanical stability of different models of Zn-Aβ-peptide complexes have been carried out that have led to the identification of a very peculiar arrangement of Zn ions and Aβ-peptides whose stability largely depends on the formation of a Zn-His-Zn bridge assisted by an unusual deprotonated imidazole ring (imidazolate). This sort of imidazolate configuration is very similar to the one it is found in Cu,Zn-SOD (see Fig. **4**) even at mild acidic conditions.

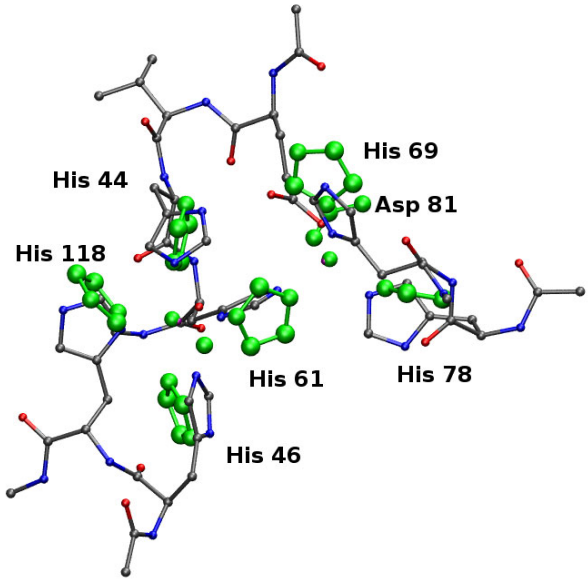

Figure 4: Comparison between S4 truncated energy-minimized model with the structure of reduced bovine SOD enzyme (PDB 1SXA) in green.

Extensive XAS studies have also been carried out on various portions of the PrP tetra-octarepeat peptide in complexes with Cu^{2+} ions, both in the presence and in the absence of Zn^{2+}. A careful analysis of these data shows that Zn acts by directly interacting with the peptide, in this way competing with Cu for binding with His. This finding suggests that metal binding competition can be important in the more general context of metal homeostasis.

Naturally the ultimate goal of the kind of complementary experimental and theoretical investigations we have illustrated in this review is to provide an understanding of the fundamental biochemical processes which are at the basis of metal metabolism, with the hope of finding new treatments for the devastating neurodegenerative diseases associated to protein aggregation and fibril formation.

ACKNOWLEDGEMENTS

We would like to thank all the many collaborators that have directly or indirectly contributed to the many of the work reported in this review. Among them special thanks are due to G. La Penna, V. Minicozzi, G.C. Rossi and F. Stellato. Fruitful discussions with F. Guerrieri and S. Furlan are also acknowledged. This work was partially supported by INFN TO61 project and PRIN project 20083Y34Y7.

CONFLICT OF INTEREST

The authors confirm that this chapter content has no conflict of interest.

DISCLOSURE

This chapter is an update of our previous publication in CAR "The Role of Metals in β-Amyloid Peptide Aggregation: X-Ray Spectroscopy and Numerical Simulations" published in 'CAR', Volume 5, Number 6, December, pp. 508 to 524.

ABBREVIATIONS

AD = Alzheimer's disease

Al = Aluminium

a.a = Amino acid

APP = Amyloid Precursor Protein

BBB = Blood Brain Barrier

CD = Circular Dichroism

CNS = Central Nervous System

CP = Car-Parrinello

CP-MD = Car-Parrinello Molecular Dynamics

Cu = Copper

DFT = Density Functional Theory

EPR = Electron Paramagnetic Resonance

EXAFS = Extended X-ray Absorption Fine Structure

Fe = Iron

fs = Femptosecond

FT = Fourier Transform

Gly = Glycine

His = Histidine

KS = Kohn and Sham

MC = Monte Carlo

MCRW = Monte Carlo Random Walk

MD = Molecular Dynamics

MDB = Metal-protein Database and Browser

MS = Multiple Scattering

NMR = Nuclear Magnetic Resonance

ns = Nanosecond

PrP = Prion Protein

ps = Picosecond

QM = Quantum-Mechanical

QM/MM = Quantum Mechanics Molecular Mechanics

SOD = Superoxide Dismutase

TSE = Transmissible Spongiform Encephalophaty

Tyr = Tyrosine

XANES = X-ray Absorption Near Edge Structure

XAS = X-ray Absorption Spectroscopy

Zn = Zinc

Appendix A

In this Appendix we recollect a few standard XAS formulae useful to recall the meaning of the physical quantities and symbols used in the text.

1) The so-called EXAFS signal, $\chi(k)$, is defined through the measured total absorption coefficient, $\mu(E)$, and the absorption coefficient of the isolated absorber, $\mu_0(E)$, *via* the relation

$$\chi(k) = \frac{\mu(E) - \mu_0(E)}{\mu_0(E)}, \quad \textbf{(1)}$$

$$\hbar k = \sqrt{2m(E - E_0)}, \quad \textbf{(2)}$$

where m is the electron mass, $\hbar$ the (reduced) Planck constant and k the wave vector of the extracted electron. The wave vector is related to the incident photon energy, E, and the ionization energy, E_0 as shown in eq. (2).

2) For completeness and to fix the notation we recall how the parameters introduced in Table **2** enter the theoretical formula representing the EXAFS signal. For simplicity we report equations valid in the single scattering approximation. In this case the theoretical EXAFS signal has the rather simple expression

$$\chi(k) = S_0^2 \sum_{\ell} \frac{N_\ell}{k r_\ell^2} \left| f_\ell(k,\pi) \right| \sin(2kr_\ell + \phi_\ell(k)) e^{-\sigma_\ell^2 k^2} e^{-2r_\ell/\lambda(k)}, \quad \textbf{(3)}$$

where the sum over ℓ runs over the different coordination shells around the absorber. N_ℓ is the number of scatterers in the ℓ-th shell, located at a distance r_ℓ from the absorber and σ_ℓ^2 is the associated Debye-Waller factor. $|f_\ell(k,\pi)|$ is the modulus of the back-scattering amplitude and $\phi_\ell(k)$ the total scattering phase. Finally S_0^2 is an empirical (positive) quantity that accounts for all the many-body losses in photo-absorption processes and $\lambda(k)$ is the photo-electron mean free path. For MS processes a formally similar expression can be derived, in which r_ℓ represents the length of the full MS path. Modulus and phase functions have now

more complicated expressions that depend on all the scattering events occurring along the MS path [38, 41-44].

3) The quality factor of a fit, *R*, is computed according to the formula

$$R = \sum_{i=1}^{P} \frac{1}{w_i} \left| \chi^{\exp}(k_i) - \chi^{th}(k_i) \right| \ , \qquad \textbf{(4)}$$

where $\chi^{\exp}(k_i)$ and $\chi^{th}(k_i)$ are the experimental and theoretical data points, respectively, and the sum is over the number, *P*, of the *k*-values at which data were collected. The "weighting" parameter w_i is given by

$$w_i = \frac{1}{k_i^n} \sum_{j=1}^{P} k_j^n \left| \chi^{\exp}(k_j) \right| \qquad \textbf{(5)}$$

where the integer *n* is selected in such a way that the amplitude of the EXAFS oscillations in the combination $k^n \left| \chi^{\exp}(k) \right|$ does not die away at large values of *k*. In the analysis presented in this work the rather standard value *n* = 3 was taken. As for the size of *R*, it is a consolidated experience that for complex biological molecules a fit can be considered adequately good when *R* takes a value that it isn't larger than 20% ÷ 40% [52].

Appendix B

In this Appendix we want to give the fundamental formulae that underlay CP-MD simulations. The CP-MD method [31, 71, 72] is based on the DFT theory the foundations of which have been laid out in the seminal papers of refs. [28, 29] (see ref. [30] for recent reviews and applications to quantum chemistry).

The N_A atoms of the system, identified by the Cartesian coordinates $\left\{\vec{R}\right\} = \left\{\vec{R}_I, I = 1, \ldots, N_A\right\}$, move (in the standard Born-Oppenheimer approximation) according to the classical equations of motion

$$M_I \frac{d^2 \vec{R}_I}{dt^2} = -\frac{\partial V_T\left(\left\{\vec{R}\right\}\right)}{\partial \vec{R}_I}, \ \ I = 1, \ldots, N_A \ , \qquad \textbf{(6)}$$

where M_I is the mass of the I-th atom and $V_T\left(\left\{\vec{R}\right\}\right)$ is the total atomic potential energy

$$V_T\left(\left\{\vec{R}\right\}\right)=\frac{1}{2}\sum_{I\neq J=1}^{N_A}\frac{Z_I Z_J e^2}{\left|\vec{R}_I-\vec{R}_J\right|}+E_{QM}\left(\left\{\vec{R}\right\}\right). \quad \textbf{(7)}$$

The first term of eq. (7) is the Coulomb potential between pairs of atoms endowed with electric charge $Z_I e$ and $Z_J e$. The second term, $E_{QM}\left(\left\{\vec{R}\right\}\right)$, is the piece of the atomic potential energy generated by the electrons according to the general principles of Quantum Mechanics. For simplicity we will assume here that the system is electrically neutral. This means that the total number of electrons, N_e, participating in the dynamics and generating the potential $E_{QM}\left(\left\{\vec{R}\right\}\right)$ is

$$N_e=\sum_{I=1}^{N_A}Z_I \quad \textbf{(8)}$$

The most difficult part of the method is the determination of $E_{QM}\left(\left\{\vec{R}\right\}\right)$. In principle this can be done by first solving the Kohn and Sham (KS) [29] equations

$$H\psi_i(\vec{r})=\varepsilon_i\psi_i(\vec{r}),\ i=1,\ldots,N_e, \quad \textbf{(9)}$$

$$H=-\frac{\hbar^2}{2m}\vec{\nabla}^2-\sum_{I=1}^{N_A}\frac{Z_I e^2}{\left|\vec{r}-\vec{R}_I\right|}+\int d\vec{r}'\,\frac{n(\vec{r}')}{\left|\vec{r}'-\vec{r}\right|}+\frac{\delta E_{xc}\left[n\right]}{\delta n(\vec{r}')}, \quad \textbf{(10)}$$

where $\vec{\nabla}^2=\partial^2/\partial x^2+\partial^2/\partial y^2+\partial^2/\partial z^2$ is the three-dimensional Laplace differential operator, $E_{xc}\left[n\right]$ is the exchange and correlation functional and $n(\vec{r})$ is the electronic density which in turn can be expressed in terms of the KS wave-functions through the formula

$$n(\vec{r})=\sum_{i=1}^{N_e}\left|\psi_i(\vec{r})\right|^2. \quad \textbf{(11)}$$

The KS equations have a precise physical meaning. They represent, in fact, the minimization condition for the following functional of the electronic density

$$E(n;\{\vec{R}\}) = -\frac{\hbar^2}{2m}\sum_{i=1}^{N_e}\int d\vec{r}\,\psi_i^{*}(\vec{r})\vec{\nabla}^2\psi_i(\vec{r}) - \int d\vec{r}\,n(\vec{r})\sum_{I=1}^{N_A}\frac{Z_I e^2}{\left|\vec{r}-\vec{R}_I\right|} + \\ + \frac{1}{2}\int d\vec{r}\int d\vec{r}^{\,'}\,\frac{n(\vec{r})n(\vec{r}^{\,'})}{\left|\vec{r}^{\,'}-\vec{r}\right|} + E_{xc}[n] \qquad \textbf{(12)}$$

Once the N_e orthonormal KS wave-functions, ψ_i, and eigenvalues, ε_i, have been determined by solving eq. (9), they can be substituted back in eq. (12) leading to the formula

$$E_{QM}(\{\vec{R}\}) = \sum_{i=1}^{N_e}\varepsilon_i - \frac{1}{2}\int d\vec{r}\int d\vec{r}^{\,'}\,\frac{n(\vec{r})n(\vec{r}^{\,'})}{\left|\vec{r}^{\,'}-\vec{r}\right|} + E_{xc}[n] - \int d\vec{r}\,\frac{\delta E_{xc}[n]}{\delta n(\vec{r})}n(\vec{r}) \ . \qquad \textbf{(13)}$$

Eq. (13) yields the desired expression of the QM atomic potential generated by the electrons appearing in eq. (7).

There are two problems with the approach we have described. The first is of a conceptual nature and has to do with the lack of a precise knowledge of the $E_{xc}[n]$ functional, which is only approximate. The second is more practical and has to do with the observation that in the way things are formulated one would have to solve the KS equations every time the atomic coordinates change as a consequence of the time evolution (6). This makes the whole procedure of simulating the dynamics of the system impossibly long and slow.

The first problem has been pragmatically solved in the literature where many, more or less sophisticated, examples of exchange and correlations functionals have been constructed in correspondence with the various specific problems that have been considered (some instances are recalled in refs. [71, 72]). The common starting point for all these formulae is the one derived from the local density approximation (LDA) equation

$$E_{xc}^{LDA}[n] = -\frac{3}{4\pi}\int d\vec{r}\,[3\pi^2 n(\vec{r})]^{1/3}n(\vec{r}) \ , \qquad \textbf{(14)}$$

that is valid in the regime of slowly varying electron density [28, 29, 94]. It may be useful to recall that the kinetic energy of a gas of free electrons is given by the following functional of the electron density

$$T^{free}[n] = \frac{3}{10}\int d\vec{r}[3\pi^2 n(\vec{r})]^{2/3} n(\vec{r}) \ . \tag{15}$$

The second problem has been brilliantly solved by Car and Parrinello in their seminal '85 paper [31]. The idea is to adiabatically move the atoms in the force field generated by the current value of the functional (12), while the latter is minimized. The minimization procedure is carried out by letting the wave functions, ψ_i, to depend on a fictitious time, *t*, and solving for the electrons the Newton-like equations of motion

$$\mu_i \frac{\partial^2 \psi_i(\vec{r},t)}{\partial t^2} = H\psi_i(\vec{r},t) - \varepsilon_i \psi_i(\vec{r},t) \ , \ i = 1,\ldots,N_e \ , \tag{16}$$

while at the same time the "electron kinetic energy", $2E_{kin} = \sum_i \mu_i \, | \, d\psi_i / dt \, |^2$ is slowly driven to zero. In eq. (14) μ_i is a parameter with the dimensions of a mass that is tuned so as to make the typical frequencies associated with the fictitious motion of the electrons of the same order of magnitude as the typical frequencies associated with the classical motion of the atoms described by eq. (6). In this way both equations can be solved employing the same time step, which for the systems of interest here turns out to be rather small, *viz*. of the order of 0.1 fs.

We conclude by observing that the set of atomic and electronic equations (eqs. (6) and (16)) can be elegantly derived from the effective Lagrangian

$$\begin{aligned} L(\{\psi\},\{\vec{R}\}) = \frac{1}{2}\sum_{I=1}^{N_A} M_I \left(\frac{d\vec{R}_I}{dt}\right)^2 + \frac{1}{2}\sum_{i=1}^{N_e} \mu_i \left|\frac{d\psi_i}{dt}\right|^2 - \frac{1}{2}\sum_{I\neq J=1}^{N_A} \frac{Z_I Z_J e^2}{\left|\vec{R}_I - \vec{R}_J\right|} + \\ - E[n;\{\vec{R}\}] + \sum_{ij=1}^{N_e} \lambda_{ij}\left(\int d\vec{r}\,\psi_j^*(\vec{r},t)\psi_i(\vec{r},t) - \delta_{ij}\right) \end{aligned} \tag{17}$$

where the last term is necessary to ensure the orthonormality of the KS wave-functions (with the ε_i in eq. (14) the eigenvalues of the symmetric matrix λ_{ij}) and the functional $E[n;\{\vec{R}\}]$ is defined in eq. (12).

REFERENCES

[1] Schläfer HL and Gliemann G. 'Basic Principles of Ligand Field Theory'. Wiley Interscience. New York (1969); Miessler GL and Tarr DA. 'Inorganic Chemistry', 3rd Ed., Pearson/Prentice Hall publisher.

[2] Bush AI. The metallobiology of Alzheimer's disease. Trends Neurosci 26: 207-214 (2003).

[3] Barnham KJ, Masters CL and Bush AI. Neurodegenerative diseases and oxidative stress. Nat Rev Drug Disc 3: 205-214 (2004).

[4] Wang H, Wang M, Li M, Chen H, Yu X, Zhao Y, Feng W, Chai Z. The distribution profile and oxidation states of biometals in APP transgenic mouse brain: dyshomeostasis with age and as a function of the development of Alzheimer's disease. Metallomics 4(3):289-296 (2012).

[5] Therry RD. The pathogenesis of Alzheimer disease: an alternative to the amyloid hypothesis. J Neuropathol Exp Neurol 55: 1023-1025 (1996).

[6] Lovell MA, Robertson JD, Teesdale WJ, Campbell JL and Markesbery WR. Copper, iron and zinc in Alzheimer's disease senile plaques. J Neurol Sci 158: 47-52 (1998).

[7] Zheng W, Aschner M and Ghersi-Egea JF. Brain barrier systems: a new frontier in metal neurotoxicological research. Toxicol Appl Pharmacol 192: 1-11 (2003).

[8] Banks WA, Kastin AJ and Zatta P. The blood-brain barrier in aluminum toxicity and Alzheimer's disease. In 'Non-neuronal cells in Alzheimer disease' (Eds: Zatta P and Nicolini M) World Scientific, Singapore, p. 1-12 (1995).

[9] Yokel RA. Brain uptake, retention, and efflux of aluminum and manganese. Environ Health Perspect (Suppl.) 5: 699-704 (2002).

[10] Bala Gupta V, Anitha S, Hedge ML, Zecca L, Garruto RM, Ravid R, Shankar SK, Stein R, Shanmugavelu P and Jagannatha Rao KS. Aluminum in Alzheimer's disease: are we still at a crossroad? Cell Mol Life Sci 62: 143-158 (2005).

[11] Drago D, Folin M, Baiguera S, Tognon G, Ricchelli F and Zatta P. Comparative effects of Aβ(1-42)-Al complex from rat and human amyloid on rat endothelial cell cultures. J Alzheimer's Dis 11: 33-44 (2007).

[12] Khan A, Ashcroft AE, Korchazhkina OV and Exley C. Metal-mediated formation of fibrillar Aβ-amyloid. J Inorg Biochem 98: 2006-2010 (2004).

[13] Morante S, González-Iglesias R, Potrich C, Meneghini C, Meyer-Klaucke W, Menestrina G, Gasset M. Inter- and intra- octarepeat Cu(II) site geometries in the prion protein. Implication in Cu(II) binding cooperativity and Cu(II)-mediated assemblies. J Biol Chem 279:11753-11759 (2004).

[14] Leal SS, Botelho HM, Gomes CM. Metal ions as modulators of protein conformation and misfolding in neurodegeneration. Coordination Chemistry available online (2012).

[15] Pepys MB. Pathogenesis, diagnosis and treatment of systemic amyloidosis. Philos Trans R Soc Lond B Biol Sci 356: 203-210 (2001).

[16] Selkoe DJ. Alzheimer's disease: genes, proteins, and therapy. Physiol Rev 81: 741-766 (2001).

[17] Cherny RA, Atwood CS, Xilinas ME, Gray DN, Jones WD, McLean CA, Barnham KJ, Volitakis I, Fraser FW, Kim YS, Huang X, Goldstein LE, Moir RD, Lim JT, Beyreuther K, Zheng H, Tanzi RE, Masters CL and Bush AI. Treatment with a copper-zinc chelator

markedly and rapidly inhibits beta-amyloid accumulation in Alzheimer's disease transgenic mice. Neurol 30: 665-676 (2001).

[18] Syme CD, Nadal RC, Rigby SEJ and Viles JH. Copper binding to the amyloid-beta (Abeta) peptide associated with Alzheimer's disease: folding, coordination geometry, pH dependence, stoichiometry, and affinity of Abeta-(1-28): insights from a range of complementary spectroscopic techniques. J Biol Chem 279: 18169-18177 (2004).

[19] Syme CD and Viles JH. Solution 1H NMR investigation of Zn2+ and Cd2+ binding to amyloid-beta peptide (Abeta) of Alzheimer's disease. Biochim Biophys Acta 1764: 246-256 (2006).

[20] Ma QF, Hu J, Wu WH, Liu HD, Du JD, Fu Y, Wu YW, Lei P, Zhao YF and Li YM. Characterization of copper binding to the peptide amyloid-beta(1-16) associated with Alzheimer's disease. Biopolymers 83: 20-31 (2006).

[21] Dong J, Shokes JE, Scott RA and Lynn DG. Modulating amyloid self-assembly and fibril morphology with Zn(II). J Am Chem Soc 128: 3540-3542 (2006).

[22] Stellato F, Menestrina G, Dalla Serra M, Potrich C, Tomazzolli R, Meyer-Klaucke W and Morante S. Metal binding in amyloid beta-peptides shows intra- and inter-peptide coordination modes. Eur Biophys J 35: 340-351 (2006).

[23] Strange RW, Blackburn NJ, Knowles PF and Hasnain SS. X-ray Absorption Spectroscopy of Metal-Histidine Coordination in Metalloproteins. Exact Simulation of the EXAFS of Tetrakis(imidazole)copper(II) Nitrate and Other Copper-Imidazole Complexes by the Use of a Multiple-Scattering Treatment. J Am Chem Soc 109: 7157-7162 (1987).

[24] Bianconi A, Di Cicco A, Pavel NV, Benfatto M, Marcelli A, Natoli CR, Pianetta P and Woicik J. Multiple-scattering effects in the K-edge x-ray-absorption near-edge structure of crystalline and amorphous silicon. Phys Rev B 36: 6426-6433 (1987).

[25] Filipponi A, Evangelisti F, Benfatto M, Mobilio S and Natoli CR. Structural investigation of a-Si and a-Si:H using x-ray-absorption spectroscopy at the Si K edge. Phys Rev B 40: 9636-9643 (1989).

[26] Zhang HH, Filipponi A, Di Cicco A, Scott MJ, Holm RH, Hedman B and Hodgson KO. Multiple-Edge XAS Studies of Cyanide-Bridged Iron-Copper Molecular Assemblies Relevant to Cyanide-Inhibited Heme-Copper Oxidases Using Four-Body Multiple-Scattering Analysis. J Am Chem Soc 119: 2470-2478 (1997) and references therein.

[27] Meneghini C and Morante S. The active site structure of tetanus neurotoxin resolved by multiple scattering analysis in X-Ray absorption spectroscopy. Biophys J 75: 1953-1963 (1998).

[28] Hohenenberg P and Kohn W. Inhomogeneous Electron Gas. Phys Rev 136: 864-871 (1964).

[29] Kohn W and Sham LJ. Quantum Density Oscillations in an Inhomogeneous Electron Gas. Phys Rev 137: 1697-1705 (1965); Kohn W and Sham LJ. Self-Consistent Equations Including Exchange and Correlation Effects. Phys Rev 140: 1133-1138 (1965).

[30] Parr RG and Yang W. 'Density Functional Theory of Atoms and Molecules'. Oxford University Press. Oxford, (1989); Dreizler RM and Gross EKU. 'Density functional theory'. Springer-Verlag, Berlin (1990); 'Primer in Density Functional Theory'. (Eds: Fiolhais C, Nogueira F and Marques MAL). Lecture Notes in Physics, Springer-Verlag, Berlin (2003).

[31] Car R and Parrinello M. Unified approach for molecular dynamics and density functional theory. Phys Rev Lett 55: 2471-2474 (1985).

[32] Giannozzi P, de Angelis F and Car R. First-principle molecular dynamics with ultrasoft pseudopotentials: parallel implementation and application to extended bio-inorganic system. J Chem Phys 120: 5903-5914 (2004).

[33] Bianconi A., Congiu-Castellano A, Dell'Ariccia M, Giovannelli A, Morante S, Burattini E and Durham PJ. 'Local Fe site structure in the tense-to-relaxed transition in carp deoxyhemoglobin: a XANES (x-ray absorption near edge structure) study'. Proc Natl Acad Sci USA 83: 7736-7740 (1986).

[34] Morante S, Gonzalez-Iglesias R, Potrich C, Meneghini C, Meyer-Klaucke W, Menestrina G and Gasset M. Inter- and intra-octarepeat Cu(II) site geometries in the prion protein: implications in Cu(II) binding cooperativity and Cu(II)-mediated assemblies. J Biol Chem 279: 11753-11759 (2004).

[35] Redecke L, Meyer-Klaucke W, Koker M, Clos J, Georgieva D, Genov N, Echner H, Kalbacher H, Perbandt M, Bredehorst R, Völter W and Betzel C. Comparative analysis of the human and chicken prion protein copper binding regions at pH 6.5. J Biol Chem 280: 13987-13992 (2005).

[36] Mentler M, Weiss A, Grantner K, Del Pino P, Deluca D, Fiori S, Renner C, Meyer-Klaucke W, Moroder L, Bertsch U, Kretzschmar HA, Tavan P and Parak FG. A New Method to determine the Structure of the Metal Environment in Metalloproteins: Investigation of the Prion Protein Octapeptide Repeat Cu(2+) Complex. Eur Biophys J 34(2): 97-112 (2005).

[37] Del Pino P, Weiss A, Bertsch U, Renner C, Mentler M, Grantner K, Fiorino F, Meyer-Klaucke W, Moroder L, Kretzschmar HA and Parak FG. The Configuration of the Cu(2+) Binding Region in Full-Length Human Prion Protein. Eur Biophys J 36: 239-252 (2007).

[38] Benfatto M, Natoli CR, Bianconi A, Garcia J, Marcelli A, Fanfoni M and Davoli I. Multiple-scattering regime and higher-order correlations in x-ray-absorption spectra of liquid solutions. Phys Rev B34: 5774-5781 (1986).

[39] Lee PA, Citrin PH, Eisenberg P and Kinkaid BM. Extended x-ray absorption fine structure: its strengths and limitations as a structural tool. Rev Mod Phys 53: 769-806 (1981).

[40] Morante S. The rôle of metals in β-amyloid peptide aggregation: X-ray spectroscopy and numerical simulations. Current Alzheimer Research 5/6: 508-524 (2008).

[41] Lee PA and Pendry JB. Theory of the extended X-ray absorption fine structure. Phys Rev 11: 2795-2811 (1975).

[42] Gurman SJ, Binsted N and Ross I. A rapid, exact, curved-wave theory for EXAFS calculations. II. The multiple-scattering contributions. J Phys C19: 1845-1861 (1986).

[43] 'X-ray Absorption. Principles, applications, techniques of EXAFS, SEXAFS and XANES'. (Eds: Koningsberger DC and Prins R) John Wiley & Sons (1988) and references quoted therein.

[44] Rehr JJ and Albers RC. Scattering-matrix formulation of curved-wave multiple-scattering theory: Application to x-ray-absorption fine structure. Phys Rev B41: 8139-8149 (1990).

[45] Benfatto M and Della Longa S. Geometrical fitting of experimental XANES spectra by a full multiple-scattering procedure. J Synchrotron Rad 8: 1087-1094 (2001).

[46] Della Longa S, Arcovito A, Girasole M, Hazemann JL and Benfatto M. Quantitative analysis of x-ray absorption near edge structure data by a full multiple scattering procedure: the Fe-CO geometry in photolysed carbonmonoxy-myoglobin single crystal. Phys Rev Lett 87: 155501-155504 (2001).

[47] Benfatto M, Della Longa S, Qin Y, Li Q, Pan G, Wu Z and Morante S. The rôle of Zn in the interplay among Langmuir-Blodgett multilayer and myelin basic protein: a quantitative analysis of XANES spectra. Biophys Chem 110: 191-201 (2004).

[48] Filipponi A, Di Cicco A and Natoli CR. X-ray-absorption spectroscopy and n-body distribution functions in condensed matter. I. Theory. Phys Rev B52: 15122-15134 (1995).

[49] Filipponi A and Di Cicco A. X-ray-absorption spectroscopy and n-body distribution functions in condensed matter. II. Data analysis and applications. Phys Rev B52: 15135-15149 (1995).

[50] Ankudinov AL, Ravel B, Rehr JJ and Conradson SD. Real Space Multiple Scattering Calculation of XANES. Phys Rev B58: 7565-7576 (1998).

[51] Binsted N, Strange RW and Hasnain SS. Constrained and restrained refinement in EXAFS data analysis with curved wave theory. Biochemistry 31: 12117-12125 (1992).

[52] Binsted N. EXCURV98: CCLRC Daresbury Laboratory computer program (1998).

[53] Rehr JJ and Albers RC. Theoretical approaches to x-ray absorption fine structure. Rev Mod Phys 72: 621-654 (2000).

[54] Bunker G, Stern EA, Blankeship RE and Parson WW. An x-ray absorption study of the iron site in bacterial photosynthetic reaction center. Biophys J 37: 539-551 (1982); Blackburn NJ, Hasnain SS, Diakun GP, Knowles PF, Binsted N and Garner CD. An extended x-ray absorption fine structure study of the copper and zinc sites of freeze-dried bovine superoxide dismutase. Biochem J 213: 765-768 (1983).

[55] Rossi GC. Theories, models, simulations: A computational challenge. e-print: arXiv: 0607211 [hep-th].

[56] Allen MP and Tildesley DJ. 'Computer Simulation of Liquids'. Clarendon Press, Oxford, UK (1990); Frenkel D and Smit B. 'Understanding Molecular Simulations'. Academic Press, San Diego, USA (1996).

[57] Martonak R, Laio A and Parrinello M. Predicting crystal structures: the Parrinello-Rahman method revisited. e-print: arXiv: 0211551 [cond-mat]; Kuo I-FW, Mundy CJ, McGrath MJ, Siepmann JI, VandeVondele J, Sprik M, Hutter J, Chen B, Klein ML, Mohamed FR, Krack M and Parrinello M. Liquid Water from First Principles: Investigation of Different Sampling Approaches. J Phys Chem B108: 12990-12998 (2004); Aktah D, Passerone D and Parrinello M. Insights into the Electronic Dynamics in Chemical Reactions. J Phys Chem A108: 848-854 (2004); Kühne TD, Krack M, Mohamed FR and Parrinello M. An Efficient and Accurate Car-Parrinello-like Approach to Born-Oppenheimer Molecular Dynamics. Phys Rev Lett 98: 066401-4 (2007).

[58] Carloni P, Blochl P and Parrinello M. Electronic structure of the Cu, Zn superoxide dismutase active site and its interactions with the substrate. J Phys Chem 99: 1338-1348 (1995); Hutter J, Carloni P and Parrinello M. Nonempirical Calculations of a Hydrated RNA Duplex. J Am Chem Soc 118: 8710-8712 (1996); Carloni P. Density Functional Theory-Based Molecular Dynamics of Biological Systems. Quant Struct Act Relat 21: 166-172 (2002); Piana S, Bucher D, Carloni P and Rothlisberger U. Reaction Mechanism of HIV-1 Protease by Hybrid Car-Parrinello/Classical MD Simulations. J Phys Chem B108: 11139-11149 (2004); Sharma M, Resta R and Car R. Intermolecular Dynamical Charge Fluctuations in Water: A Signature of the H-Bond Network. Phys Rev Lett 95: 187401-4 (2005).

[59] Furlan S, La Penna G, Guerrieri F, Morante S and Rossi GC. *Ab initio* simulations of Cu binding sites on the N-terminal region of prion protein. J Biol Inorg Chem 12: 571-583 (2007).

[60] Furlan S, La Penna G, Guerrieri F, Morante S and Rossi GC. Studying the Cu binding sites in the PrP N-terminal region: a test case for *ab initio* simulations. Eur Biophys J 36: 841-845 (2007).

[61] Ewald PP. Die Berechnung optischer und elektrostatischer Gitterpotentiale. Ann Phys 64: 253-287 (1921); Allen MP and Tildesley DJ. 'Computer simulation of liquids'. Clarendon Press, New York (1988); Darden T, York D and Pedersen L. Particle mesh Ewald: An N-log(N) method for Ewald sums in large systems. J Chem Phys 98: 10089-10092 (1993); Essmann U, Perera L, Berkowitz ML, Darden T, Lee H and Pedersen LG. A smooth particle mesh Ewald potential. J Chem Phys 103: 8577-8592 (1995).

[62] Gao J. Review on QM/MM. Reviews in Comp Chem 7: 119-185 (1996); Assfeld X and Rivail JL. Quantum chemical computations on parts of large molecules: The ab initio Local Self-Consistent Field method. Chem Phys Lett 263: 100-106 (1996); Bash PA, Ho LL, MacKerell ADJ, Levine D and Hallstrom P. Progress toward chemical accuracy in the computer simulation of condensed phase reactions. Proc Natl Acad Sci 93 3698-3703 (1996); Field MJ, Bash PA and Karplus M. A Combined Quantum Mechanical and Molecular Mechanical Potential for Molecular Dynamics Simulations. J Comp Chem 11: 700-733 (1990); Freindorf M and Gao J. Optimization of the Lennard-Jones Parameter for Combined Ab Initio Quantum Mechanical and Molecular Mechanical Potential Using the 3-21G Basis Set. J Comp Chem 17: 386-395 (1996); Gao J. Hybrid Quantum and Molecular Mechanical Simulations: An Alternative Avenue to Solvent Effects in Organic Chemistry. Acc Chem Res 29: 298-305 (1996); Eichinger M, Tavan P, Hutter J and Parrinello M. A hybrid method for solutes in complex solvents: density functional theory combined with empirical force fields. J Chem Phys 110: 10452-10467; Reuter N, Dejaegere A, Maigret B. and Karplus M. Frontier Bonds in QM/MM Methods: A Comparison of Different Methods. J Phys Chem A104 1720-1735 (2000).

[63] Lambert MP, Barlow AK, Chromy BA, Edwards C, Freed R, Liosatos M, Morgan TE, Rozovsky I, Trommer B, Viola KL, Wals P, Zhang C, Finch CE, Krafft GA and Klein WL. Diffusible, nonfibrillar ligands derived from Abeta-42 are potent central nervous system neurotoxins. Proc Natl Acad Sci USA 95: 6448-6453 (1998).

[64] Chromy BA, Nowak RJ, Lambert MP, Viola KL, Chang L, Velasco PT, Jones BW, Fernandez SJ, Lacor PN, Horowitz P, Finch CE, Krafft GA and Klein WL. Self-assembly of Abeta (1-42) into globular neurotoxins. Biochemistry 42: 12749-12760 (2003).

[65] Klein WL. Cytotoxic intermediates in the fibrillation pathway: Aβ-oligomers in Alzheimer's disease as a case study. In 'Protein Misfolding, Aggregation and Conformational diseases. Part A' (Eds: Uversky VN and Fink AL) p. 61-81 Springer-Verlag, Berlin (2006).

[66] Baroni S, Dal Corso A, de Gironcoli S, Giannozzi P, Cavazzoni C, Ballabio G, Scandolo S, Chiarotti G, Focher P, Pasquarello A, Laasonen K, Trave A, Car R, Marzari N and Kokalj A. http://www.pwscf.org/.

[67] Van der Spoel D, van Buuren AR, Apol E, Meulenhoff PJ, Tieleman DP, Sijbers ALTM, Hess B, Feenstra KA, Lindhal E, van Drunen R and Berensden HJC. 'Gromacs User Manual' version 3.1.1; Nijenborgh 4, 9747 AG Groningen: The Netherlands, 2002; http://www.gromacs.org.

[68] http://amber.scripps.edu/

[69] Nosé S. A molecular dynamics method for simulations in the canonical ensemble. Molec Phys 52: 255-268 (1984); Hoover WG. Canonical dynamics: equilibrium phase-space distributions. Phys Rev A 31: 1695-1697 (1985).

[70] Frenkel D and Smit B. 'Understanding molecular simulation' Academic Press, San Diego (1996).

[71] Payne MC, Teter MP, Allan DC, Arias TA and Joannopoulos JD. Iterative minimization techniques for ab initio total-energy calculations: molecular dynamics and conjugate gradients. Rev Mod Phys 64: 1045-1097 (1992).

[72] Mark D and Hutter J. in 'Modern Methods and Algorithms of Quantum Chemistry' (Ed. Grotendorst J.), John von Neumann Institute for Computing, Jülich, http://www.fz-juelich.de/nic-series.

[73] http://www.embl.org/

[74] Minicozzi V, Stellato F, Comai M, Dalla Serra M, Potrich C, Meyer-Klaucke W and Morante S. Identifying the minimal Cu and Zn binding site sequence in Amyloid beta peptides. J Biol Chem 283: 10784-10792 (2008).

[75] Zirah S, Kozin SA, Mazur AK, Blond A, Cheminant M, Ségalas-Milazzo I, Debey P and Rebuffat S. Structural Changes of Region 1-16 of the Alzheimer Disease Amyloid-Peptide upon Zinc Binding and *in Vitro* Aging. J Biol Chem 281: 2151-2161 (2006).

[76] Danielsson J, Pierattelli R, Banci L and Graslund A. High-resolution NMR studies of the zinc-binding site of the Alzheimer's amyloid beta-peptide. FEBS J 274: 46-59 (2007).

[77] Castagnetto JM, Hennessy SW, Roberts VA, Getzoff ED, Tainer JA and Pique ME. MDB: the Metalloprotein Database and Browser at The Scripps Research Institute. Nucleic Acids Res 30: 379-382 (2002).

[78] Kowalik-Jankowska T, Ruta M, Wisniewska K and Lankiewicz L. Coordination abilities of the 1-16 and 1-28 fragments of β-amyloid peptide towards copper(II) ions: a combined potentiometric and spectroscopic study. J Inorg Biochem 95: 270-282 (2003).

[79] Miura T, Suzuki K, Kohata N and Takeuchi H. Metal Binding Modes of Alzheimer's Amyloid β-Peptide in Insoluble Aggregates and Soluble Complexes. Biochemistry 39: 7024-7031 (2000).

[80] Kirschner DA, Abraham C and Selkoe DJ. X-ray diffraction from intraneuronal paired helical filaments and extraneuronal amyloid fibers in Alzheimer disease indicates cross-β conformation. Proc Natl Acad Sci USA 83: 503-507 (1986); Kirschner DA, Inouye H, Duffy LK, Sinclair A, Lind M and Selkoe DJ. Synthetic peptide homologous to β protein from Alzheimer disease forms amyloid-like fibrils *in vitro*. Proc Natl Acad Sci USA 84: 6953-6957 (1987); Sunde M, Serpell LC, Bartlam M, Fraser PE, Bepys MB and Blake CCF. Common core structure of amyloid fibrils by synchrotron x-ray diffraction. J Mol Biol 273: 729-739 (1997); Balbach JJ, Ishii Y, Antzutkin ON, Leapman RD, Rizzo NW, Dyda F, Reed J and Tycko R. Amyloid fibril formation by $A\beta_{16-22}$, a seven-residue fragment of the Alzheimer's β-amyloid peptide, and structural characterization by solid state NMR. Biochemistry 39: 13748-13759 (2000).

[81] Ma B and Nussinov R. Stabilities and conformations of Alzheimers β -amyloid peptide oligomers ($A\beta_{16-22}$, $A\beta_{16-35}$ and $A\beta_{10-35}$: sequence effects. Proc Natl Acad Sci USA 99: 14126-14131 (2002); Rohrig UF, Laio A, Tantalo N, Parrinello M and Petronzio R. Stability and structure of oligomers of the Alzheimer peptide $A\beta_{16-22}$: From the dimer to the 32-mer. Biophys J 91: 3217-3229 (2006).

[82] Tickler AK, Smith DG, Ciccotosto GD, Tew DJ, Curtain CC, Carrington D, Masters CL, Bush AI, Cherny RA, Cappa R, Wade JD, Barnham KJ. Methylation of the imidazole side chains of the Alzheimer disease amyloid-beta peptide results in abolition of superoxide dismutase-like structures and inhibition of neurotoxicity. J Biol Chem 280: 13355-13363 (2005).

[83] Minicozzi V, Morante S, Rossi GC, Stellato F, Christian N, Jansen K. The rôle of metals in aggregation. Experiments and *ab initio* simulations. Int J Q Chem 108: 1992-2015 (2008).
[84] Karr JW, Akintoye H, Kaupp LJ, Szalai VA. N-terminal deletions modify the Cu^{2+} binding site in amyloid-beta. Biochemistry 44: 5478-5487 (2005).
[85] Karr JW, Szalai VA. Role of aspartate-1 in Cu(II) binding to the amyloid-beta peptide of Alzheimer's disease. J Am Chem Soc 129: 3796-3797 (2007).
[86] Frank P, Benfatto M, Hedman B, Hodgson KO. The X-ray Absorption Spectroscopic model of the Copper (II) imidazole complex ion in liquid aqueous solution: a strongly solvated square pyramid. Inorganic Chemistry 51: 2086-2096 (2012).
[87] Frank P, Benfatto M, Szilagyi RK, D'Angelo P, Della Longa S, Hodgson KO. The Solution Structure of $[Cu(aq)]^{2+}$ and Its Implications for Rack-Induced Bonding in Blue Copper Protein Active Sites. Inorg Chem 44: 1922-1933 (2005).
[88] Frank P, Benfatto M, Hedman B, Hodgson KO. Solution $[Cu(amm)]^{2+}$ is a strongly solvated square pyramid: a full account of the copper K-edge XAS spectrum within single-electron theory. Inorg Chem 47: 4126-4139 (2008).
[89] Atwood CS, Moir RD, Huang X, Scarpa RC, Bacarra NM, Romano DM, Hartshorn MA, Tanzi RE, Bush AI. Dramatic aggregation of Alzheimer abeta by Cu(II) is induced by conditions representing physiological acidosis. J Biol Chem 273: 12817-12826 (1998).
[90] Atwood CS, Scarpa RC, Huang X, Moir RD, Jones WD, Fairlie DP, Tanzi RE, Bush AI. Characterization of copper interactions with alzheimer amyloid beta peptides: identification of an attomolar-affinity copper binding site on amyloid beta1-42. J Neurochem 75: 1219-1233 (2000).
[91] Faller P, Hureau C. Bioinorganic chemistry of copper and zinc ions coordinated to amyloid-beta peptide. Dalton Trans 21:1080-1094 (2009).
[92] Mantri Y, Fioroni M, Baik MH. Computational study of the binding of CuII to Alzheimer's amyloid-beta peptide: do Abeta42 and Abeta40 bind copper in identical fashion? J Biol Inorg Chem 13:1197-1204 (2009).
[93] Raffa DF, Gomez-Balderas R, Brunelle P, Rickard GA, Rauk A. Ab initio model studies of copper binding to peptides containing a His-His sequence: relevance to the beta-amyloid peptide of Alzheimer's disease. J Biol Inorg Chem 10: 887-902 (2005).
[94] Furlan S, La Penna G. Modeling of the Zn2+ binding in the 1-16 region of the amyloid beta peptide involved in Alzheimer's disease. Phys Chem Chem Phys 11: 6468-6481 (2009).
[95] Peters MB, Yang Y, Wang B, Füsti-Molnár L, Weaver MN, Merz KMJ. Structural Survey of Zinc Containing Proteins and the Development of the Zinc AMBER Force Field (ZAFF). J Chem Theory Comput 6: 2935-2947 (2010).
[96] Siebert X, Eipper BA, Mains RE, Prigge S, Blackburn NJ, Amzel LM. The catalytic copper of peptidylglycine alpha-hydroxylating monooxygenase also plays a critical structural role. Biophys J 89: 3312-3319 (2005).
[97] Strange RW, Antonyuk SV, Hough MA, Doucette PA, Valentine JS, Hasnain SS. Variable metallation of human superoxide dismutase: atomic resolution crystal structures of Cu-Zn, Zn-Zn and as-isolated wild-type enzymes. J Mol Biol 356:1152-1162 (2006).
[98] Allen FH. The Cambridge Structural Database: a quarter of a million crystal structures and rising. Acta Crystallogr Sect. B: Struct Sci. 58: 380-388 (2002).
[99] Giannozzi P, Jansen K, La Penna G, Minicozzi V, Morante S, Rossi GC, Stellato F. Proving metal involvement in beta-amyloid aggregation by ab-initio simulations and XAS measurements. Metallomics 4(2):156-165 (2012).

[100] La Penna G, Morante S, Perico A, Rossi GC. Designing generalized statistical ensembles for numerical simulations of biopolymers. J Chem Phys 121:10725-10741 (2004).
[101] Jorgensen WL, Chandrasekhar J, Madura JD, Impey RW, Klein MJ. Comparison of simple potential functions for simulating liquid water. J Chem Phys 79: 926-935 (1983).
[102] Minicozzi V, Morante S. Is Cu involved in prion oligopeptide stability? Experiments and numerical simulations. Int J Quantum Chem 110: 656-680(2010).